ISSN: 2165-3259

JAOCR

Official Journal of the American Osteopathic College of Radiology

AOCR ANNUAL MEETING EXHIBITS



Guest Editor: Donald von Borstel, D.O.

Editor-in-Chief: Daniel J. Wale, D.O.

July 2020, Vol. 9, Issue 3

JAOCR

Official Journal of the American Osteopathic College of Radiology

Aims and Scope

The Journal of the American Osteopathic College of Radiology (JAOCR) is designed to provide practical up-to-date reviews of critical topics in radiology for practicing radiologists and radiology trainees. Each quarterly issue covers a particular radiology subspecialty and is composed of high-quality review articles and case reports that highlight differential diagnoses and important teaching points.

Access to Articles

All articles published in the JAOCR are open access online. Subscriptions to the journal are not required to view or download articles. Reprints are not available.

Copyrights

Materials published in the JAOCR are protected by copyright. No part of this publication may be reproduced without written permission from the AOCR.

Guide for Authors

Submissions for the JAOCR are by invitation only. If you were invited to submit an article and have questions regarding the content or format, please contact the appropriate Guest Editor for that particular issue. Although contributions are invited, they are subject to peer review and final acceptance.

Editor-in-Chief

Daniel J. Wale, D.O., Ann Arbor, MI

Editor Emeritus

William T. O'Brien, Sr., D.O., Cincinnati, OH

Editorial Board

Abdominal/Body Radiology
Sharon A. Kreuer, D.O., Monroeville, PA
Rocky C. Saenz, D.O., F.A.O.C.R., Farmington Hills, MI

Breast Radiology
Matthew Tommack, D.O., Eugene, OR
Michelle C. Walters, D.O., Dallas, TX

Chest and Cardiac Radiology
Mark Guelfguat, D.O., Bronx, NY
Douglas Johnson, D.O., Charlotte, NC

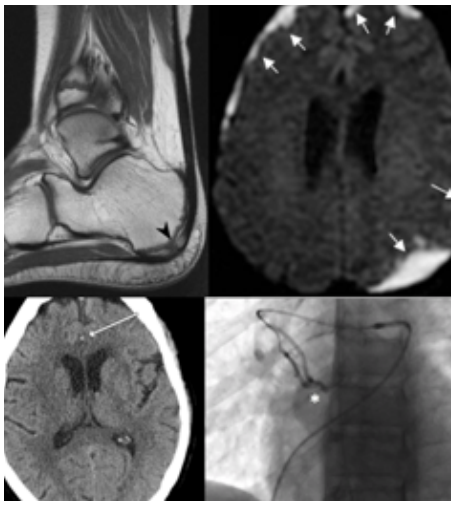
Musculoskeletal Radiology
Christopher Cerniglia, D.O., M.Eng., Westborough, MA
Matthew Tommack, D.O., Eugene, OR
Donald von Borstel, D.O., Tulsa, OK

Neuroradiology
Robert Koenigsberg, D.O., F.A.O.C.R., Philadelphia, PA
Alysha Vartevan, D.O., Scottsdale, AZ

Nuclear Medicine
Timothy McKnight, D.O., Farmington Hills, MI
Daniel J. Wale, D.O., Ann Arbor, MI

Pediatric Radiology
Brooke S. Lampl, D.O., Cleveland, OH
Emily Janitz, D.O., Akron, OH

Vascular and Interventional Radiology
Aaron T. Rucks, D.O., M.S., Erie, PA



JAOCR

ANNUAL EXHIBITS

Guest Editor: Donald von Borstel, D.O.

From the Editor

In this Issue 4
Donald von Borstel, D.O.

Review Articles

Overcoming Your Achilles Heel: A Review of Achilles Tendon Anatomy, Pathology and Associated MRI Findings 5
David Young, D.O., Colby DeGiacomo, D.O., Sarah Fisher, D.O., Donald von Borstel, D.O.

MRI of Sports-related Injuries in Adolescent Athletes 14
Avik Patel, D.O., Harris Shaikh, D.O., Robert Selley, D.O., Kevin Carter, D.O.

Decoding the Diffusion: Overview of Restricted Diffusion on Brain MRI 20
Jeremy Daniel, D.O., Yoon Cho, D.O., Donald von Borstel, D.O., Kyle Summers, D.O.

JAOCR at the Viewbox

Hyperdense Bihemispheric Anterior Cerebral Artery: An Uncommon Location of a Classic Imaging Finding 32
Alex Martin, D.O., Timothy McKnight, D.O.

Hereditary Hemorrhagic Telangiectasia: A Review 33
Mathieu Sabbagh, D.O., Donald von Borstel, D.O.



"Life is like riding a bicycle. To keep your balance, you must keep moving."

—

Albert Einstein

In this Issue

Donald von Borstel, D.O.

Subspecialty Chief of the Musculoskeletal Division and Residency Program Director
Oklahoma State University Center for Health Sciences, Tulsa, OK

I would like to thank Editor-in-Chief Dr. Wale and the JAOCR for allowing me to serve as guest editor for this issue. This issue of the JAOCR is intended to highlight the Annual Exhibits presented at the 2019 AOCR Annual Meeting. The top Annual Exhibits submitted to the conference were invited for submission to this issue, highlighting the involved residents and their institutions.

As the topics chosen were the top Annual Exhibits from the AOCR annual conference, they cover a broad range. The first review article covers the MRI appearance and pathology of the Achilles tendon and surrounding structures. The residents at OSU Center for Health Sciences Drs. Young, Fisher, and DeGiacomo were instrumental in producing this article. Our goal is to assist the general radiologist in accurately describing Achilles tendon injuries and related pathology.

The second review article was written by Drs. Patel, Shaikh, Selley, and Carter from the Department of Radiology at Michigan State University and McLaren Healthcare. This is an overview of the most common sports-related injuries in adolescent athletes. Radiologists play a key role in identifying patterns of overuse injury in adolescent athletes and can have a significant impact on initiation of treatment.

Our last review article was written by residents and faculty at OSU Center for Health Sciences Drs. Daniel, Cho, and Summers. This article focuses on the differential considerations for restricted diffusion on brain MRI with excellent imaging representations of a multitude of etiologies.

Our Viewbox articles were from the Annual Exhibits presented by Dr. Sabbagh at the University of Arkansas Department of Interventional Radiology, and Dr. Martin who is a resident at the Beaumont Health - Farmington Hills Department of Radiology.

Thank you to all the authors and their essential contributions. I hope this issue entices radiology residents, faculty, and practicing radiologists to attend the AOCR meetings in the future and submit their research and educational material for future Annual Exhibits. Lastly and most importantly, thank you to my wife for her continued love and support through everything!

Overcoming Your Achilles Heel: A Review of Achilles Tendon Anatomy, Pathology and Associated MRI Findings

David Young, D.O., Colby Degiacomo, D.O., Sarah Fisher, D.O., Donald von Borstel, D.O.

Department of Radiology, Oklahoma State University Center for Health Sciences, Tulsa, OK

The Achilles tendon is among the most frequently injured tendons despite it being the strongest and largest tendon in the body.[1] Achilles tendon injuries are common in both athletes and nonathletes, often resulting from predisposing factors such as mechanical injury (repetitive loading), vascular disease, corticosteroids, quinolone antibiotics, inflammatory arthropathies, autoimmune illnesses, hyperpronation, diabetes mellitus, and gout.[2]

This article will briefly review the anatomy of the Achilles tendon and discuss the different pathologies and their associated MRI findings.

Anatomy

The Achilles tendon is the strongest tendon in the human body. Its action provides plantar flexion and, to a lesser degree, knee flexion.[1] The Achilles tendon is a common tendon shared by the gastrocnemius and soleus muscles with its distal insertion at the posterosuperior aspect of the calcaneus.

The Achilles tendon is made up of numerous fascicular bundles enclosed almost completely within a paratenon.[3,4] The paratenon serves a similar function to synovium, providing nutrition to the tendon. Because the Achilles tendon has a single axis of motion, there is no need for the lubricating function of synovium.[5,6] There is diminished blood supply to the tendon 2 to 6 cm proximal to the calcaneal insertion where the mesotendal vascular anastomosis blood supply is decreased. This portion of the Achilles tendon is called the "critical zone." This is the most common location for Achilles tendon rupture.[7] Distal tears are uncommon because of the blood supplied from the calcaneal insertion periosteal vessels.[5,7] Adjacent structures include the Kager fat pad, which is anterior to the Achilles tendon, and the retrocalcaneal (RC) bursa. The RC bursa is a 1- to 2-cm synovial reflection interposed between the posterior surface of the calcaneus and the Kager's fat pad anterior surface of the distal Achilles (**Figure 1**).

The Achilles tendon normally has low-signal intensity on all imaging sequences. On axial images, the anterior margin of the Achilles is concave for most of its course (**Figure 2**). An exception would be at the soleus insertion where the margin is typically convex and may be focally bulbous.[5] The normal fascicular anatomy may be visible as a linear signal on T1-weighted and proton density (PD)-weighted sequences but is not as readily apparent on T2-weighted images (T1WI) (**Figure 3**). Punctate areas of increased signal can be seen in the distal tendon on axial images representing interfascicular septa containing intratendinous vessels. Also, the anatomic course of the tendon fibers can result in imaging artifact (magic angle effect) on short echo time (TE) sequences. This is generally less well-defined and unlikely to be punctate or linear in morphology.[3,6] On sagittal images, the anterior and posterior margins of the Achilles tendon should be parallel below the soleus insertion. On coronal images, the margins of the tendon should be fairly straight with the tendon widening distally.[8]

Tendinosis

Achilles tendinopathy is a broad term describing pathology of the tendon. This can include both tendonitis and tendinosis; however, it is commonly used to describe insertional disease such as insertional tendinopathy. Tendinosis is a more specific term describing noninflammatory degeneration of the tendon, often resulting from repetitive microtrauma, either at the Achilles insertion or midsubstance.[6] Tendinosis is the most common abnormality involving the midsubstance of the Achilles tendon and is most often acute in onset and proximal to the RC bursa. This entity usually occurs in older individuals who are less active and overweight.[8,9] Conversely, insertional tendinopathy occurs typically in a middle-aged athlete who presents following an increase in training duration, intensity, and frequency with pain in the mid portion of the tendon.[10]

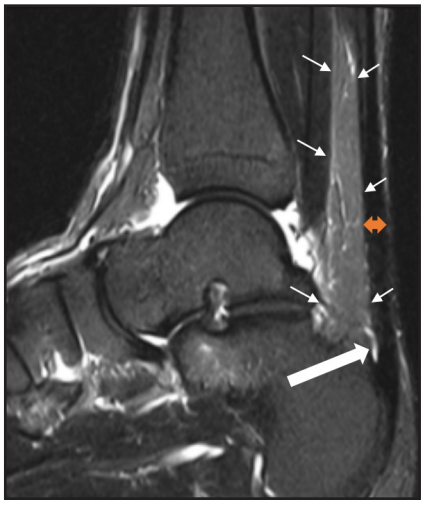


FIGURE 1. *Normal hindfoot anatomy. Sagittal T2-weighted, fat-saturated image showing normal thickness of the Achilles tendon (orange arrow). The normal Kager's fat pad is demonstrated (white arrows) along with visualization of normal fluid-signal in the retrocalcaneal bursa (long arrow).*

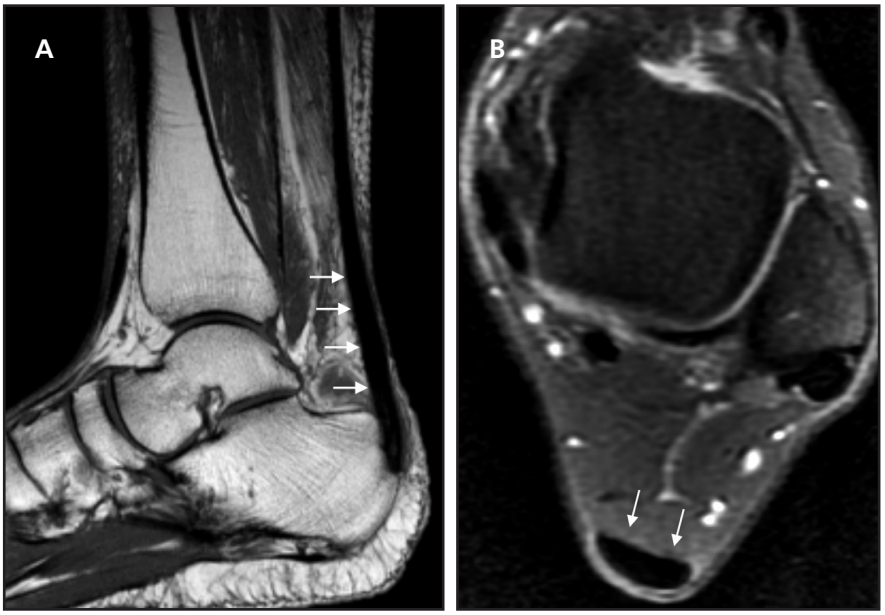


FIGURE 2. *Normal Achilles. Sagittal T1WI (A) showing normal anatomy and positioning of the Achilles tendon (arrows). Axial PD-weighted, fat-saturated image (B) showing normal concave anterior contour of the Achilles tendon (arrow).*

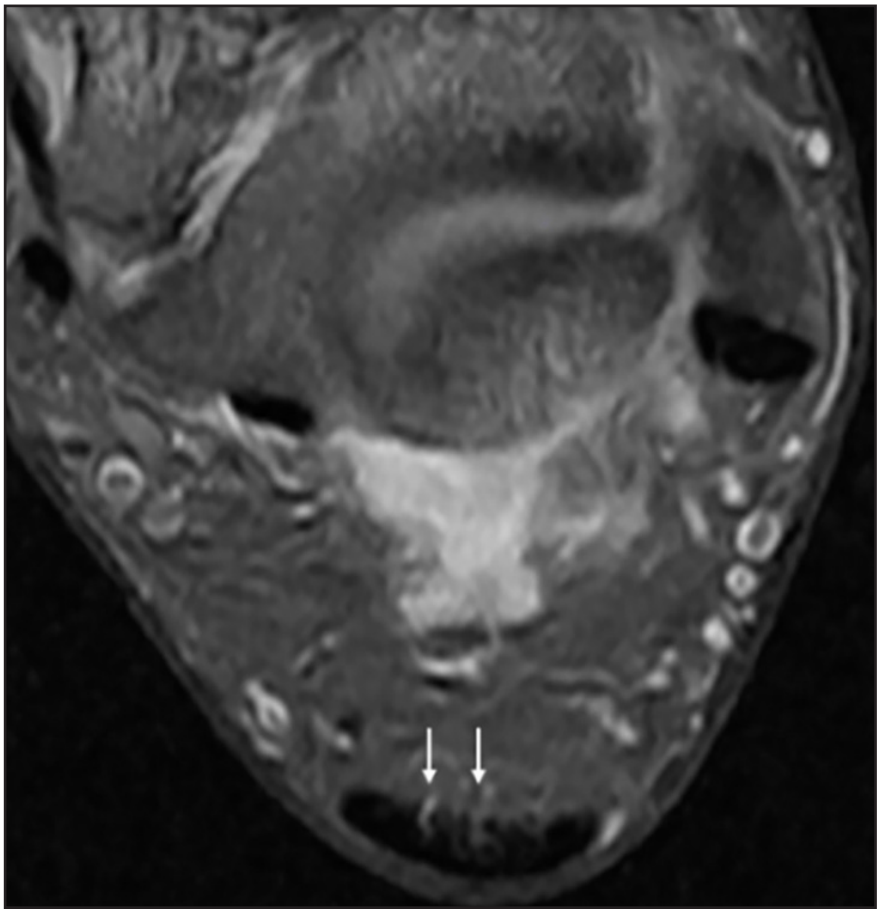


FIGURE 3. *Normal anterior linear signal in the Achilles tendon. Axial PD-weighted, fat-saturated image of the Achilles tendon demonstrating normal anterior linear signal variations (arrows) that should not be mistaken for a tear/injury.*

Histologically, findings of intratendinous mucoid or fatty degeneration are present with a disorganized collagen structure. This tendinous degeneration can progress to stages of microtears, intrasubstance tear, partial tears, and complete tears.[11] Underlying hypoxic degenerative tendinopathy is commonly seen in patients who have acutely ruptured Achilles tendons. These hypoxic changes are likely caused by ischemia due to the relative hypovascularity of the Achilles tendon critical zone with secondary overuse or repetitive microtrauma resulting in a thickened, dysmorphic Achilles tendon 2 to 6 cm proximal to the calcaneal insertion.[12,13]

MRI will show a thickened tendon > 8 mm in anteroposterior (AP) dimension with an anterior convexity of the tendon contour (**Figure 4**).[5,8] Intermediate T2-weighted signal secondary to the mucoid deposits or interstitial tearing may be seen. This intermediate signal intensity suggests that a chronic process exists, in contrast to a hyperintense "fluid-like" signal, suggesting an acute component.[6]

Partial Tear

A partial tear of the Achilles is defined as an incomplete disruption of the tendon fibers, often extending to the tendon



FIGURE 4. *(A) Tendinosis. Sagittal T1WI demonstrating mildly thickened Achilles tendon (arrow). (B) Tendinosis. Axial STIR images demonstrating Achilles tendon with convex anterior contour (arrow).*



FIGURE 5. *Sagittal PD-fat saturated sequence with an acute partial tear of the Achilles tendon undersurface demonstrating hyperintense signal at the location of the tear (arrow).*



FIGURE 6. *Complete tear. Sagittal PD fat-saturated image of the ankle displaying a complete midsubstance tear of the Achilles tendon (yellow arrow).*

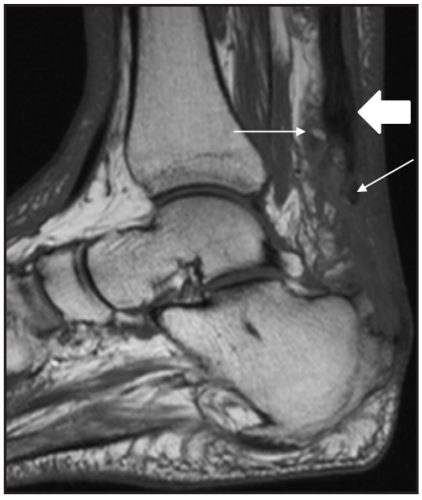


FIGURE 7. *Complete tear. Sagittal T1WI of a complete Achilles tendon tear with multiple avulsion fragments (thin arrows) attached to the hypointense retracted tendon stump (thick arrow).*

surface. Partial tears can occur anywhere along the Achilles tendon, but are most common in the critical zone.[14] On MRI, partial tears demonstrate alteration in architecture with interruption of tendon fibers. Hyperintense signal on fluid-sensitive sequences and hypointense signal on T1-weighted images (T1WIs) demonstrate the tear (**Figure 5**).[15,16] Chronic Achilles tendon tears demonstrate intermediate signal intensity on fluid-sensitive sequences with a thickened tendon. The tendon edges will be retracted and there may be ongoing atrophy of the Achilles tendon fibers and muscle.[17]

Muscle atrophy can be a manifestation of a chronic tendon tear, with irreversible atrophy presenting as a fatty infiltrated or "marbled" muscle.[5,16] Atrophy occurs first in the soleus because of the predominance of slow-twitch fibers. Because the soleus muscle is part of the Achilles tendon unit, soleus atrophy can be thought of as a predictor of a dysfunctional myotendinous unit. Therefore, when imaging the Achilles tendon, sagittal images should include at least 3 cm of the distal soleus muscle belly to assess for fatty infiltration of the muscle. Gastrocnemius atrophy can be seen but is rare.[5,16]

Treatment typically consists of initial nonsurgical management such as casting, nonweightbearing, and functional bracing. Platelet-rich plasma injections have been proposed for refractory cases

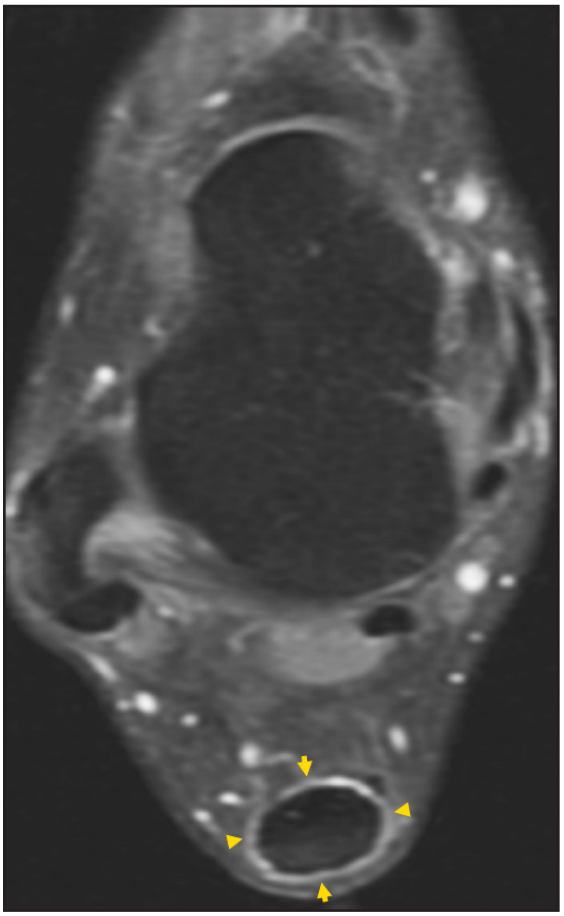


FIGURE 8. *Peritendinitis/Paratenonitis. Axial T1-weighted, fat-saturated postcontrast image demonstrating circumferential enhancement and inflammation of the paratenon (orange arrowheads) with superimposed tendinosis of the Achilles, which is thickened with an anterior convex contour.*

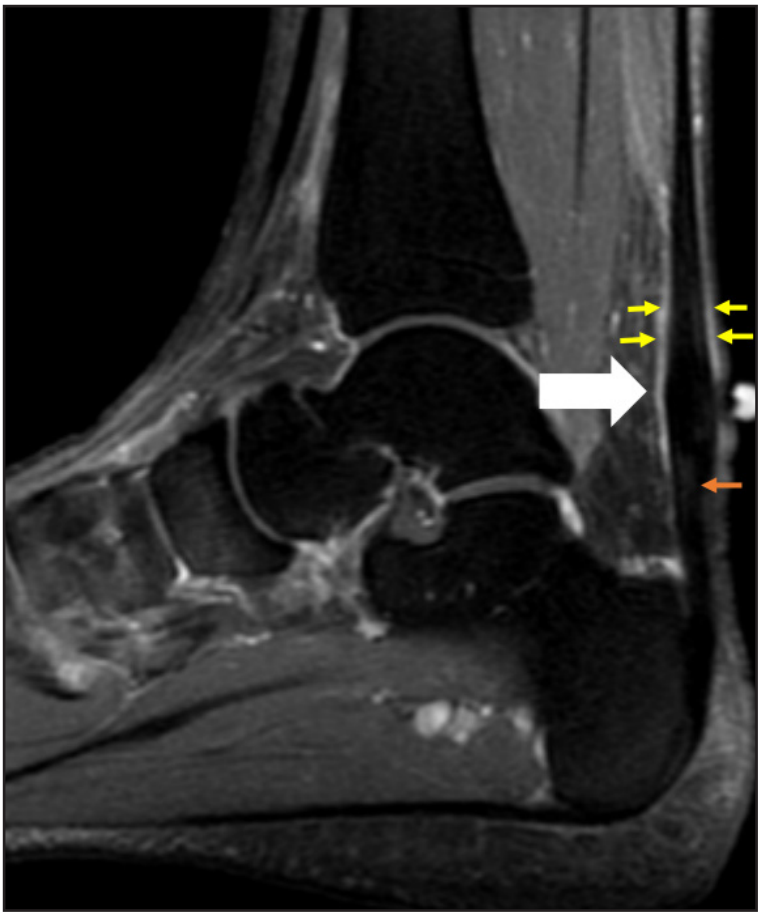


FIGURE 9. *Tendinitis. Sagittal T1-weighted fat-saturated postcontrast image demonstrating ill-defined longitudinal signal within the distal tendon (orange arrow). Notice there is also peritendinitis (yellow arrows) and thickening of the Achilles tendon with localized abnormal contour (thick white arrow).*

of tendinopathy, with evidence supporting efficacy of these Achilles injections.[17] If conservative management fails, an open or percutaneous surgery may be performed.[18,19]

Complete Tear

Achilles ruptures, or a full-thickness tear involving the entire width of the tendon, are defined as a complete discontinuity of the tendon. Complete tears occur in a bimodal distribution in individuals aged 25 to 40 years and those older than 60.[6] The mechanism leading to rupture is not fully understood; however, some pathological factors are known such as activities that require a dorsiflexed position while running or jumping, degenerative changes, recurrent microtrauma, corticosteroids, fluoroquinolone use, chronic renal failure, rheumatoid arthritis, and systemic lupus erythematosus.[2]

Complete tears will demonstrate a T2-weighted hyperintense signal defect of the tendon with fluid-signal or a heterogeneous signal hematoma filling the tendon gap. The torn tendon fibers are commonly distracted or overlapping (**Figure 6**).[14] T1WI will demonstrate a hypointense stump just above the fluid-filled gap and is also useful to visualize potential avulsed osseous fragments (**Figure 7**). These avulsion fractures are best seen on x-ray, highlighting one of the many important reasons MRI interpretation should be done with an available x-ray correlation. Of note, the size of the tendon gap, quality of the torn tendon, estimation of cross-sectional involvement, and presence of atrophy of the soleus and gastrocnemius muscles are useful descriptors for the surgeon and should be recorded in the radiology report.[16]

Treatment remains controversial. In general, operative treatment allows improved functional outcome with greater likelihood of returning to the same performance level and decreased repeat rupture rate in athletes.[6] The possibility of surgical complications and the greater cost are the obvious disadvantages. Nonoperative management has a greater likelihood of patient dissatisfaction and outcomes are heavily dependent on patient compliance to the rehabilitation protocol.[2]

Peritendinitis

Peritendinitis, also referred to as "paratenonitis," is defined as an

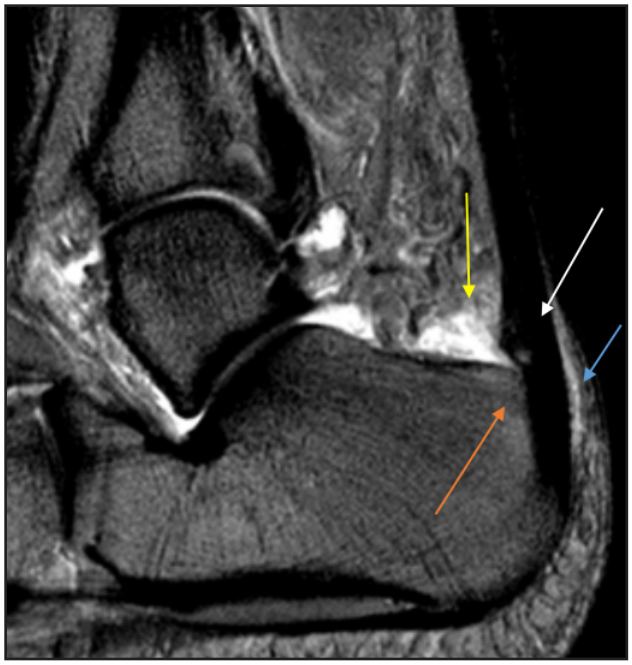


FIGURE 10. *Haglund's syndrome. Sagittal STIR image demonstrating retro-Achilles (blue) and retrocalcaneal (yellow arrow) bursitis. Osseous prominence of the posterosuperior calcaneus (orange arrow) and tendinopathy (white arrow).*



FIGURE 11. *Haglund's syndrome. Sagittal PD-weighted, fat-saturated image demonstrates an osseous prominence at the posterosuperior calcaneus (dashed arrow), retrocalcaneal bursitis (solid arrow) and partial-thickness undersurface tear of the Achilles (arrowhead).*

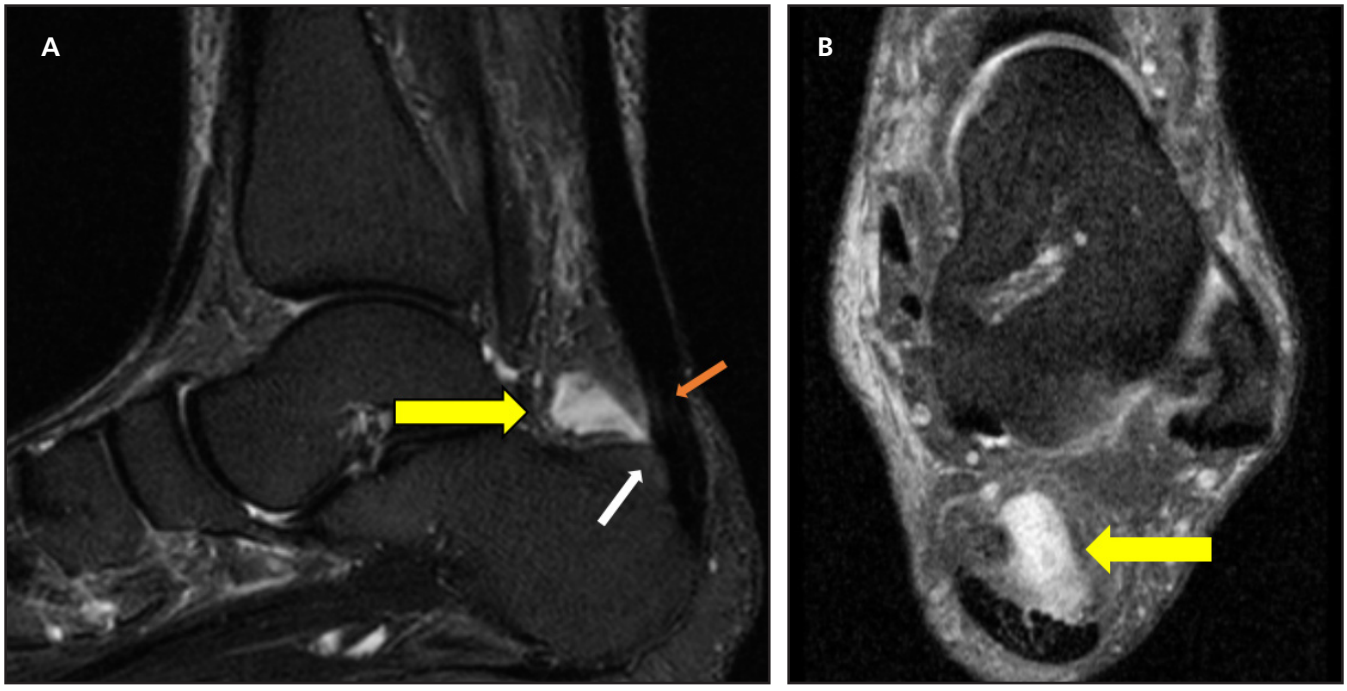


FIGURE 12. *Retrocalcaneal bursitis. (A) Sagittal STIR image demonstrating enlarged RC bursa with hyperintense fluid-signal. Additional findings of insertional tendinopathy (orange arrow) and a prominent posterosuperior calcaneus tuberosity (white arrow) complete the triad of Haglund's syndrome. (B) Axial PD-weighted, fat-saturated image shows enlarged RC bursa with hyperintense fluid-signal.*

inflammatory condition of the paratenon surrounding the tendon and is most commonly seen in active athletes due to repetitive overuse injuries. It can also arise from disorders such as seronegative arthritis and infection.[20] On MRI this presents with hyperintense T2-weighted and short-TI inversion recovery (STIR) signal surrounding the Achilles tendon (**Figure 8**). Additionally, in the acute phase, fluid-signal may be seen between the tendon and the paratenon, and inflammatory changes commonly extend into the subcutaneous fat and Kager fat pad.[8]

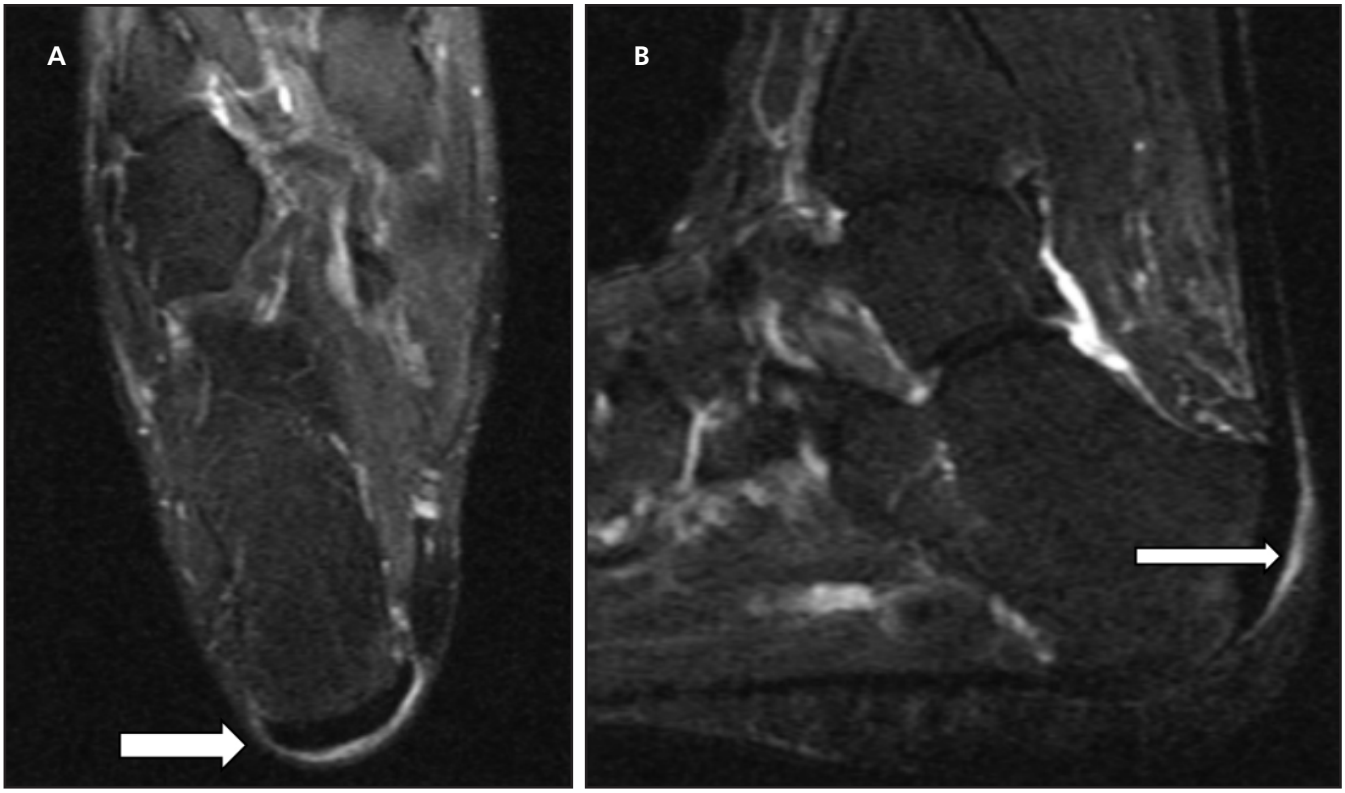


FIGURE 13. *Retro-Achilles bursitis. Axial T2-weighted, fat-saturated (A) and sagittal STIR (B) images of the heel demonstrating hyperintense signal within the retro-Achilleal bursa (arrows).*

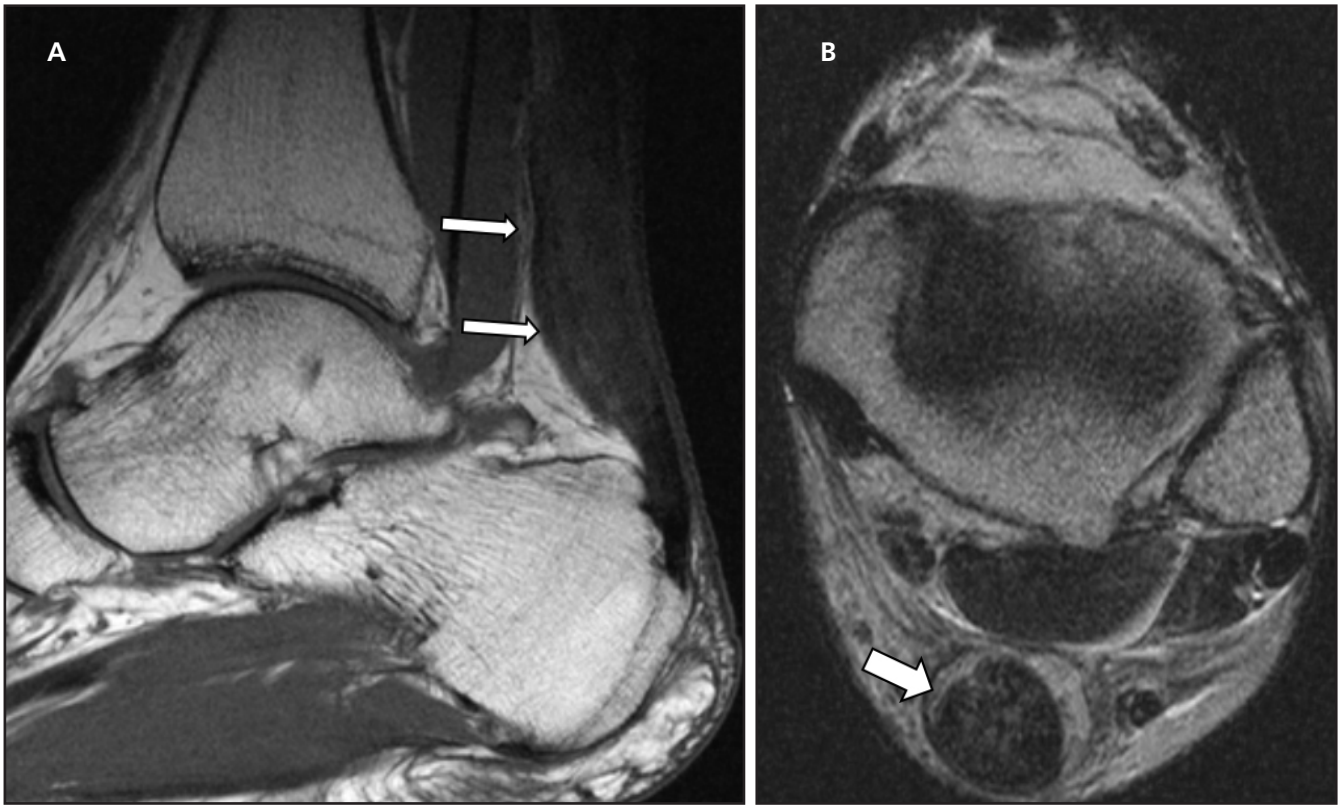


FIGURE 14. *(A and B) Achilles xanthoma. Sagittal (A) and Axial (B) T1WIs demonstrating intermediate signal intensity between tendon bundles creating a "speckled" appearance of the Achilles tendon (solid arrows).*

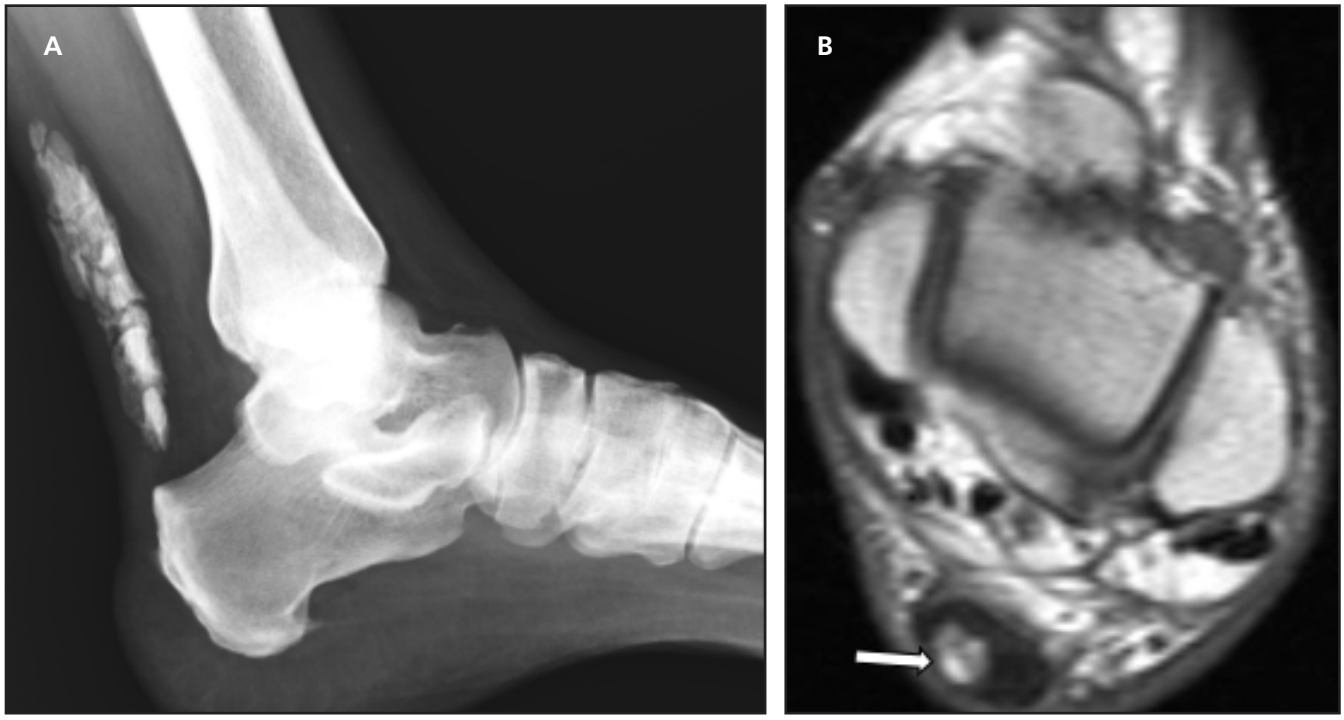


FIGURE 15. *Ossification. Lateral view of ankle (A) demonstrates ossified Achilles tendon (solid arrows). Axial T1WI (B) demonstrates a structure isointense to marrow within the Achilles tendon (solid arrow).*

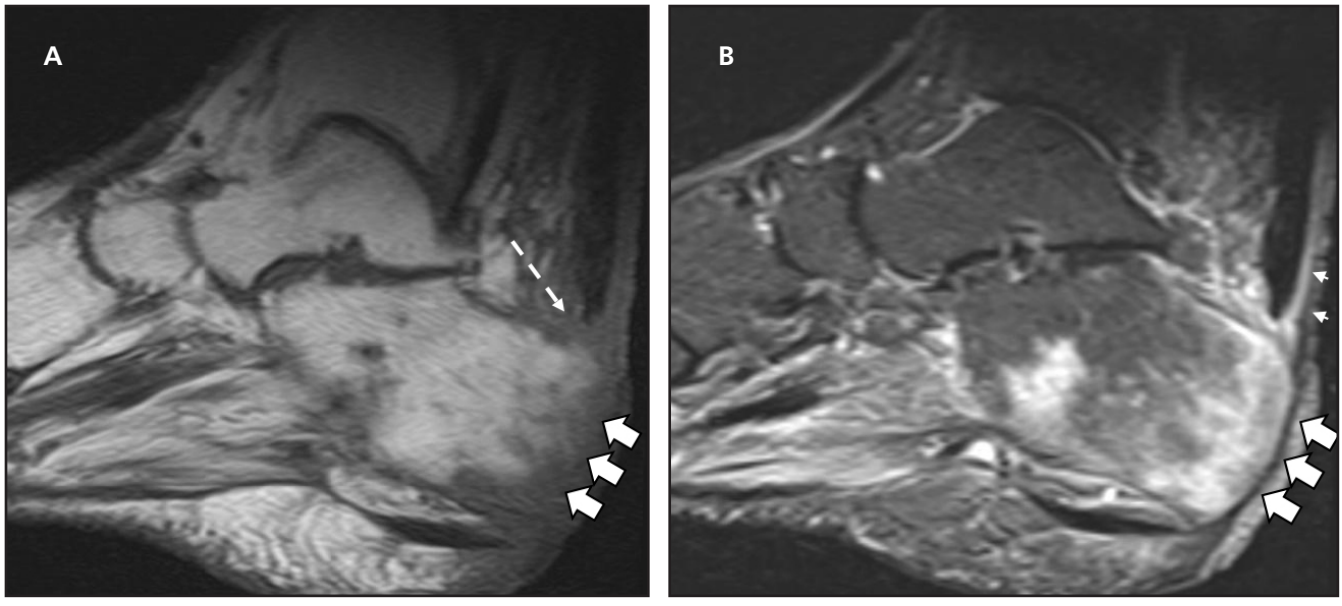


FIGURE 16. *Infection. Sagittal T1WI (A) and T2 fat-saturated images demonstrate a large posterior heel wound with osteomyelitis (solid arrows) and a full-thickness Achilles tendon tear at the attachment to the infected calcaneus (dashed arrow) with surrounding peritendinitis (arrowheads).*

Tendinitis

Tendinitis is most commonly located at the distal tendon calcaneal insertion and frequently coexists with adjacent soft-tissue and osseous pathology. It is common in runners and frequently leads to the development of a calcaneal enthesophyte.[21]

MRI demonstrates thickening of the distal tendon with vague, ill-defined longitudinal T1-weighted postcontrast, T2-weighted, and STIR hyperintense signal (**Figure 9**). This signal may be intense and can mimic a partial tear, albeit fairly distally. Edema within enthesophytes correlates with more acute symptoms.[21] RC bursitis is a frequent accompanying finding.

Tendinitis and peritendinitis usually respond to nonsurgical measures including rest, ice, compression, training modifications, NSAIDs, heel lifts, orthotics, and night splints.[2] Local injections of pharmacologic agents have not

proven efficacious. In recalcitrant cases of peritendinitis, brisement (injection of fluid between the tendon and the paratenon) has been advocated.[6]

Haglund Syndrome

Haglund deformity is a somewhat common cause of heel pain that predominantly affects middle-aged women and is often bilateral. It was first documented in 1927 by Swedish orthopedist Patrick Haglund. While it is largely considered idiopathic, there are several known contributing factors.[22] For instance, the Haglund deformity is also known as the "pump bump." The "pump" refers to the low-back, high-heeled shoes commonly associated, and the "bump" refers to the prominent calcaneal projection that results.[14] Other common causes include repetitive use or chronic stress such as excessive running, poor biomechanics due to cavovarus deformities, or a stiff heel-counter of footwear (eg, dress shoe) that can compress the bursa against the calcaneus.[23]

The posterior calcaneal tuberosity serves as a partial site of attachment for the Achilles tendon as it extends down the posterior calcaneus. The RC bursa cushions the tendon from the tuberosity. When exposed to chronic stress over time, the posterosuperior aspect of the tuberosity hypertrophies resulting in a Haglund deformity.[14] Eventually this results in a cycle of painful inflammation of the RC bursa and Achilles tendon known as Haglund syndrome.[24]

In general, lateral radiographs will show a bony projection along the posterosuperior aspect of the calcaneal tuberosity. MRI will show excess fluid in the RC and retro-Achilles bursae on STIR and T2WI as well as bone marrow edema in the hypertrophied calcaneal tuberosity.[14] (**Figures 10 and 11**).

First-line treatment of symptoms associated with Haglund's syndrome is typically nonsurgical, such as wearing appropriate footwear and orthotics, reducing activity, stretching the gastrocnemius and soleus, and taking NSAIDs. If nonsurgical treatment fails, the recommended procedures include surgical osteotomy with removal of the superolateral deformity and calcaneal step with decompression of the RC bursa.[24]

Retrocalcaneal and Retro-Achilles Bursitis

The RC bursa is a saddle-shaped structure that is deep to the Achilles tendon and its paratenon and is posterosuperior to the posterior calcaneal tubercle and Kager's fat pad. RC bursitis is most commonly due to repetitive trauma and is frequently found in runners. Other causes include rheumatoid arthritis and seronegative spondyloarthropathies.[14] Normal-sized RC bursa on asymptomatic patients measures approximately 1 mm (AP) x 6 mm (transverse) x 3 mm (craniocaudal).[24] There is measurable T2-weighted and STIR hyperintense fluid signal on MRI. In symptomatic patients, the RC bursae will typically measure > 1 mm AP x 11 mm transverse x 7 mm craniocaudal.[25]

When the bursa is enlarged with fluid it will obscure the RC fat.[26] Therefore, the presence of the RC recess on lateral plantar flexion radiographs essentially excludes the possibility of RC bursitis. On plain film, RC bursitis can be diagnosed by a normal Achilles tendon, normal superficial soft tissues, and normal calcaneal cortex in the setting of an obliterated RC recess.[27]

An enlarged bursa with hypointense T1-weighted and hyperintense fluid-sensitive signal is a key finding on MRI (**Figure 12**).[14] Some studies suggest that an AP measurement > 2 mm seen on MRI may be considered diagnostic for RC bursitis. However, in some chronic cases, fibrosis and scarring may eventually shrink the inflamed bursa, making the dimensions inconsistent with the diagnosis.[25]

Resection of the posterosuperior aspect of the calcaneus has been shown to be up to 92% effective in treating RC bursitis if performed within 1 year of symptom onset, but the most common treatment is corticosteroid injections.[28]

The retro-Achilles bursa is located between the Achilles tendon and the skin. Inflammation usually is caused by repetitive trauma/irritation from the posterior heel counter of a shoe. MR imaging demonstrates hyperintense signal posterior to the Achilles tendon on a fluid-sensitive sequence (**Figure 13**).[29] As with RC bursitis, treatment is typically nonsurgical with progression to corticosteroid injections if necessary.

Achilles Xanthoma

Achilles xanthoma is a reactive lesion due to hyperlipoproteinemia most commonly found in the Achilles tendon. It is often painless and slow growing and will cause diffuse tendon enlargement over time. MRI demonstrates intermediate T1-weighted, STIR, and T2-weighted signal between low-signal tendon bundles. There may be a speckled appearance on axial images (**Figure 14**).[30]

Atypical Achilles Pathologies

Ossification of the Achilles Tendon

On a macroscopic level in the Achilles, tendon ossification occurs more frequently than tendon calcification and is relatively more common in the Achilles than in other tendons in the body. Nevertheless, it is a rare condition that is usually associated with prior surgery or history of repetitive running-related tendonitis. Tendon ossification predominates distally in the tendon, appearing as focal fatty marrow. It will demonstrate the same signal as bone on MRI and may have an appearance of a fractured enthesophyte (**Figure 15**).[31]

Infection

Infection of the Achilles tendon occurs most often in people with diabetes and vasculopathy from postsurgical complications and more commonly direct extension of calcaneal osteomyelitis from heel ulcers.[32] In the setting of osteomyelitis, the distal aspect of the tendon is most commonly involved due to proximity with the overlying soft-tissue infection (**Figure 16**). Contrast enhancement of the Achilles tendon and the presence of peritendinous fluid-signal on T2WI are not specific for the presence of a tendon infection; these

findings can also be seen in patients with inflammatory conditions, degenerative disorders of the tendons, and in patients who have sustained trauma. However, circular enhancement of a tendon passing through an area of cellulitis from an infected pedal ulcer may be a specific sign of infection.[33,34]

Conclusion

Achilles tendon injuries are common and increasing in frequency due to their association with an aging and active population. Having a firm understanding of the normal anatomy and pathology of the Achilles tendon with the associated MRI findings is paramount in helping guide the clinician to a more accurate diagnosis and earlier treatment for patients.

References

1. O'Brien M. Functional anatomy and physiology of tendons. Clin Sports Med 1992;11(3):505-520.
2. Uquillas CA, Guss MS, Ryan DJ, Jazrawi LM, Strauss EJ. Everything Achilles: knowledge update and current concepts in management: AAOS exhibit selection. J Bone Joint Surg 2015;97(14):1187-1195.
3. Mantel D, Flautre B, Bastian D, Delforge PM, Delvalle A, Leclet H. Structural MRI study of the Achilles tendon. Correlation with microanatomy and histology. J Radiol 1996;77(4):261-265.
4. Cheney D, Smith C, Brooks D, et al. An overview of hindfoot pain and MRI findings. J Am Osteopath Coll Radiol 2019;8(4):11-17.
5. Schweitzer ME, Karasick D. MR imaging of disorders of the Achilles tendon. Am J Roentgenol 2000;175(3):613-625.
6. Stadnick ME. Achilles Tendon Pathology. MRI Web Clinic. Radsource. Published January 3, 2017. Accessed March 7, 2020. http://radsource.us/achilles-tendon-pathology/
7. Lagergren C, Lindholm A. Vascular distribution in the Achilles tendon: an angiographic and microangiographic study. Acta Chir Scand 1959;116:491-495.
8. Irwin TA. Current concepts review: insertional Achilles tendinopathy. Foot Ankle Int 2010;31(10):933-939.
9. Chimenti RL, Cychosz CC, Hall MM, Phisitkul P. Current concepts review update: insertional Achilles tendinopathy. Foot Ankle Int 2017;38(10):1160-1169.
10. Narváez JA, Narváez J, Ortega R, Aguilera C, Sánchez A, Andía E. Painful heel: MR imaging findings. RadioGraphics 2000;20(2):333-352.
11. Paavola M, Kannus P, Järvinen TAH, Khan K, Józsa L, Järvinen M. Achilles tendinopathy. J Bone Joint Surg Am 2002;84-A(11):2062-2076.
12. Leach RE, Dilorio E, Harney RA. Pathologic hindfoot conditions in the athlete. Clin Orthop Relat Res 1983;177:116-121.
13. Kannus P, Jozsa L. Histopathological changes preceding spontaneous rupture of a tendon. J Bone Joint Surg Am 1991;73(10):1507-1525.
14. Lawrence DA, Rolen MF, Abi Morshed K, Moukaddam H, Moukaddam H. MRI of heel pain. Am J Roentgenol 2013;200:845-855.
15. Astrom M, Gentz CF, Nilsson P, Rausing A, Sjoberg S, Westlin N. Imaging in chronic Achilles tendinopathy: a comparison of ultrasonography, magnetic resonance imaging and surgical findings in 27 histologically verified cases. Skeletal Radiol 1996;25:615-620.
16. Pierre-Jerome C, Moncayo V, Terk MR. MRI of the Achilles tendon: a comprehensive review of the anatomy, biomechanics, and imaging of overuse tendinopathies. Acta Radiol 2010;51(4):438-454.
17. Oloff L, Elmi E, Nelson J, Crain J. Retrospective analysis of the effectiveness of platelet-rich plasma in the treatment of Achilles tendinopathy: pretreatment and posttreatment correlation of magnetic resonance imaging and clinical assessment. Foot Ankle Spec 2015;8(6):490-497. doi:10.1177/1938640015599033
18. Haggmark T, Liedberg H, Erikson E, Wredmark T. Calf muscle atrophy and muscle function after non-operative versus operative treatment of Achilles tendon ruptures. Orthopedics 1986;9:160-164.
19. Saleh M, Marshall PD, Senior R, MacFarlane A. The Sheffield splint for controlled early mobilization after rupture of the calcaneal tendon. A prospective, randomized comparison with plaster treatment. J Bone Joint Surg Br 1992;74(2):206-209.
20. Schepsis A, Jones H, Haas AL. Achilles tendon disorders in athletes. Am J Sports Med 2002;30(2):287-305.
21. Kang S, Thordarson DB, Charlton TP. Insertional Achilles tendinitis and Haglund's deformity. Foot Ankle Int 2012;33(6):487-491.
22. Vaishya R, Agarwal AK, Azizi AT, Vigay V. Haglund's syndrome: a commonly seen mysterious condition. 2016 Cureus 8(10):e820.
23. Stephens MM. Haglund's deformity and retrocalcaneal bursitis. Orthop Clin North Am 1994;25(1),41-46.
24. Sella EJ, Caminear DS, McLarney EA. Haglund's syndrome. J Foot Ankle Surg 1998;37(2),110-114.
25. Bottger BA, Schweitzer ME, El-Noueam KI, Desai M. MR imaging of the normal and abnormal retrocalcaneal bursae. Am J Roentgenol 1998;170(5):1239-1241.
26. Canoso JJ, Liu N, Traill MR, et al. Physiology of the retrocalcaneal bursa. Ann Rheumatic Dis 1988;47: 910-912.
27. Heneghan MA, Wallace T. Heel pain due to retrocalcaneal bursitis: radiographic diagnosis (with a historical footnote on Sever's disease). Pediatr Radiol 1985;15:119-122.
28. Angermann, P. Chronic retrocalcaneal bursitis treated by resection of the calcaneus. Foot Ankle. 1990;10(5):285-287.
29. Luck MD, Gordon AG, Blebea JS, Dalinka MK. High association between accessory soleus muscle and Achilles tendonopathy. Skeletal Radiol 2008;37(12):1129-1133.
30. Rodriguez CP, Goyal M, Wasdahl D. Best cases from the AFIP: atypical imaging features of bilateral Achilles tendon xanthomatosis. RadioGraphics 2008;28(7):2064-2068.
31. Lotke PA. Ossification of the Achilles tendon: report of seven cases. J Bone Joint Surg Am 1970;52-A:157-160.
32. Feibel RJ, Jackson RL, Lineaweaver WC, Buncke HJ. Management of chronic Achilles tendon infection with musculotendinous gracilis interposition free-flap coverage. J Reconstr Microsurg 1993;9(5): 321-325.
33. Boutin RD, Brossmann J, Sartoris DJ, Resnick D. Update on imaging of orthopedic infections. Orthop Clin North Am 1998;29:41-66.
34. Ledermann HP, Morrison WB, Schweitzer ME, Raikin SM. Tendon involvement in pedal infection: MR analysis of frequency, distribution, and spread of infection. Am J Roentgenol 2002;179:4, 939-947.

MRI of Sports-related Injuries in Adolescent Athletes

Avik Patel, D.O.,[1,2] Harris Shaikh, D.O.,[1,2] Robert Selley, D.O.,[2] Kevin Carter, D.O.[2]

[1]Department of Radiology, Michigan State University, East Lansing, MI
[2]McLaren Healthcare Network, MI

Sports participation is a contributing factor in the physical and emotional development of children while promoting habitual exercise and combating childhood obesity. Adolescent participation in sports is increasing with earlier adoption of intense training regimens and repetitive specialized motions. Concurrently, the incidence of sports-related overuse injuries is on the rise.[1]

The dynamic nature of the adolescent skeleton results in unique growth-related patterns of injury. The mainstay of treatment in all cases is suspension of activity in conjunction with physical therapy. If left undiagnosed, these injuries can lead to developmental abnormalities that increase susceptibility to future injury. Radiologists play a key role in identifying patterns of overuse injury in adolescent athletes, which facilitates the initiation of a treatment plan. It is imperative that the reviewing radiologist be familiar with associated imaging to avoid misdiagnosis and any subsequent, unnecessary intervention. MRI offers superior sensitivity and specificity compared with other imaging modalities and does not use ionizing radiation, which is essential in the adolescent athlete patient population.

Apophysitis

Apophyses serve as attachment sites for tendons and ligaments in the developing skeleton. Arising from separate ossification centers, apophyses eventually fuse with adjacent bone at variable ages, depending on location. Traction injury to this anchoring bony outgrowth is described as apophysitis.

Management is usually nonsurgical, with activity limitation and subsequent graduated rehabilitation of utmost importance. Nonsteroidal anti-inflammatory drugs are effective for pain relief. Barring potential displacement of an avulsion fracture, prognosis is typically excellent. Enlargement of an inflamed apophysis should not be mistaken for more aggressive entities, and awareness of the MRI appearance of developing musculoskeletal anatomy allows for accurate diagnosis.

Apophysitis of the Knee: Osgood-Schlatter and Sinding-Larsen-Johansson Diseases

Apophysitis of the tibial tubercle (Osgood-Schlatter) and inferior patellar pole (Sinding-Larsen-Johansson) are exceedingly common overuse injuries in adolescent athletes who routinely perform running, jumping or cutting motions. In either case, presentation may be bilateral or unilateral and males are more commonly affected. Tibial tubercle ossification occurs from proximal and distal ossification centers, which are separated by residual epiphyseal cartilage. Unfused ossification centers should not be mistaken for avulsion fracture or tibial tubercle apophysitis. The tibial tubercle apophysis is radiographically evident around age 10, with fusion typically occurring at ages 14 to 18.[2] The tubercle tethers the quadriceps muscles via the patellar tendon and undergoes traction during knee extension and hip flexion.

Osgood-Schlatter disease manifests with gradual onset cyclic pain, swelling and deformity at the tibial tubercle. An association with patella alta has been proposed. MRI will reveal marrow edema of the tibial tubercle, edema within Hoffa's fat pad, deep infrapatellar bursal fluid, and thickening of the distal patellar tendon (**Figure 1**). Displaced/nondisplaced cartilaginous and/or osseous fragmentation at the tubercle has also been described.[2]

Traction injury occurring at the patellar attachment of the patellar tendon is known as Sinding-Larsen-Johansson disease. Pain and swelling is localized to the inferior patellar pole. This is easily discernible from Osgood-Schlatter disease by the presence of proximal patellar tendinosis. MRI will reveal a thickened proximal patellar tendon and edema-like signal of the inferior patella and adjacent Hoffa fat pad. Patellar sleeve fracture and symptomatic bipartite patella can present similarly and should be excluded. Persistent pain after growth plate closure in either Osgood-Schlatter or Sinding-Larsen-Johansson disease may be due to a residual ossicle, which can be surgically excised.[2]

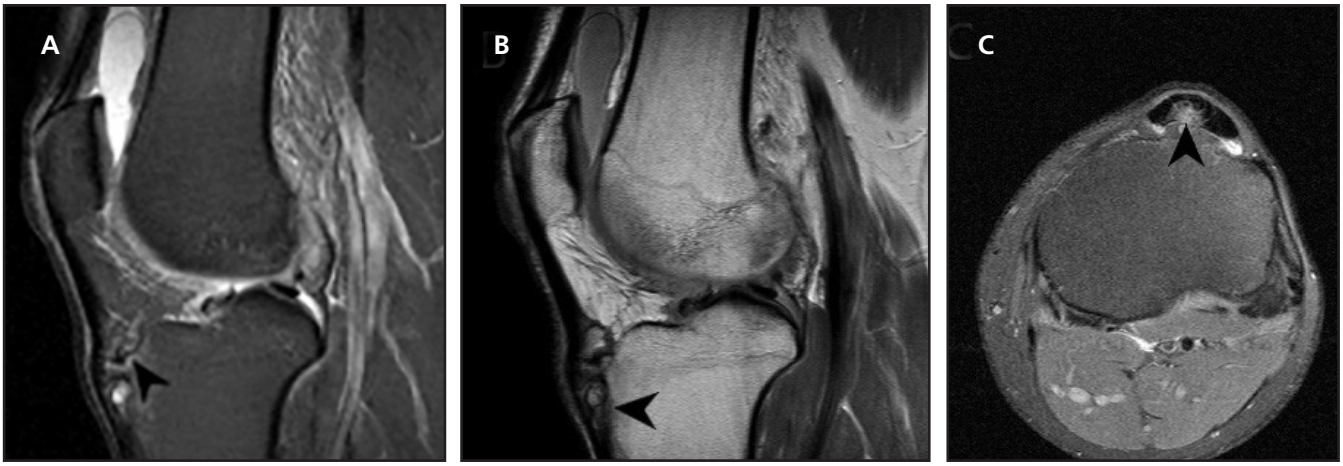


FIGURE 1. *Osgood-Schlatter disease. Sagittal fluid-sensitive MR image (A) demonstrating deep infrapatellar bursal heterogeneous signal (arrowhead) consistent with chronic bursitis. The Sagittal PD image (B) demonstrates fragmentation of the tibial tubercle (arrowhead). Axial fluid-sensitive MR image (C) demonstrating "edema-like" signal within the distal patellar tendon (arrowhead).*

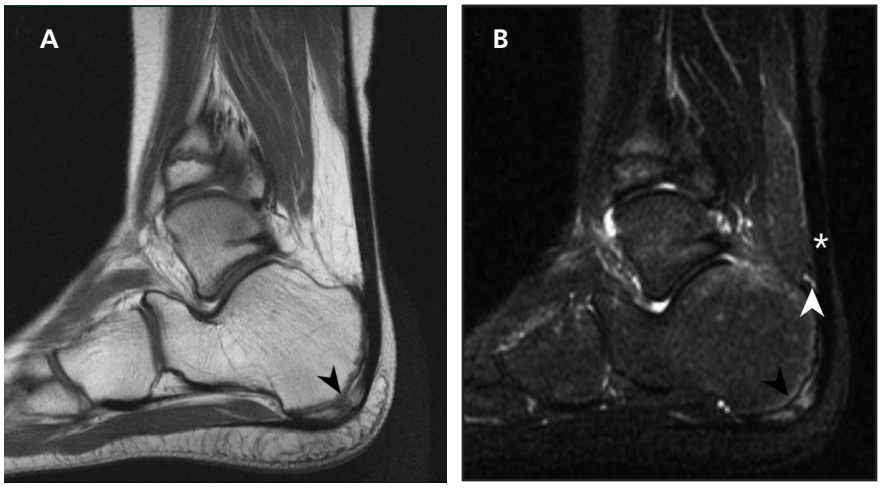


FIGURE 2. *Calcaneal apophysitis. Sagittal T1 image (A) demonstrating an irregular physeal contour and a fragmented calcaneal apophysis (arrowhead). Sagittal fluid-sensitive MR image (B) demonstrating calcaneal and apophyseal marrow edema (black arrowhead). The retrocalcaneal bursa has a normal physiologic fluid-signal (white arrowhead) and the Achilles tendon is normal in appearance (asterisk).*

Calcaneal Apophysitis: Severs Disease

The calcaneal apophysis is radiographically evident around age 7 with fusion occurring around age 16.[2] The posterior calcaneal apophysis serves as the attachment site for the gastrocnemius and soleus muscles via the Achilles tendon and undergoes traction during plantar flexion and knee flexion. Inferiorly, the plantar fascia also originates from this apophysis. Clinical presentation is typically bilateral or unilateral posterior heel pain aggravated by compression of the Achilles tendon (squeeze test). MRI will reveal apophyseal and subjacent bone marrow edema. Fragmentation and/or irregularity along the apophyseal margin may be present (**Figure 2**). Calcaneal fracture and osteomyelitis should be excluded as these can clinically mimic apophysitis.

Ischial Tuberosity Apophysitis

The ischial tuberosity apophysis is radiographically evident around age 14 with fusion typically occurring between ages 18 and 20.[2] The ischial tuberosity serves as the attachment site for the common hamstring tendon, which includes the long head of the biceps femoris, semitendinosus, and semimembranosus tendons. The biceps femoris and semitendinosus muscles combine as the conjoint tendon, which inserts on the transverse facet of the tuberosity posteromedially. Superolaterally, the semimembranosus muscle originates from the oblique facet of the tuberosity.

Traction at the apophysis occurs with repeated flexion at the knee and extension at the hip. Ischial tuberosity apophysitis is seen commonly in dancers and runners. Clinical presentation is dull hip pain that is aggravated by activity, manual compression, or isometric hamstring contraction. MRI will reveal apophyseal and subjacent bone marrow edema (**Figure 3**). Linear, hypointense signal on T1-weighted imaging (T1WI) corresponding to a nondisplaced fracture line may be evident.[3] Of note, the ischial tuberosity is the most common site of osseous avulsion in the pelvis. If displaced by at least 2 cm, an avulsed osseous fragment should be surgically fixated.[3]

Medial Epicondyle Apophysitis: Little Leaguer's Elbow

The medial epicondyle apophysis is radiographically evident at age 6 and fuses around age 15.[4] The common forearm flexors and ulnar collateral ligament attach to the medial epicondyle, which undergoes tensile stress during overhead throwing. During the late-cocking and acceleration phases of throwing, a valgus stress is generated at the elbow joint causing lateral compression and medial tension.[4] In



FIGURE 3. *Ischial tuberosity apophysitis. Coronal fluid-sensitive MR image demonstrating hyperintense signal at the left ischial tuberosity (arrowhead)*

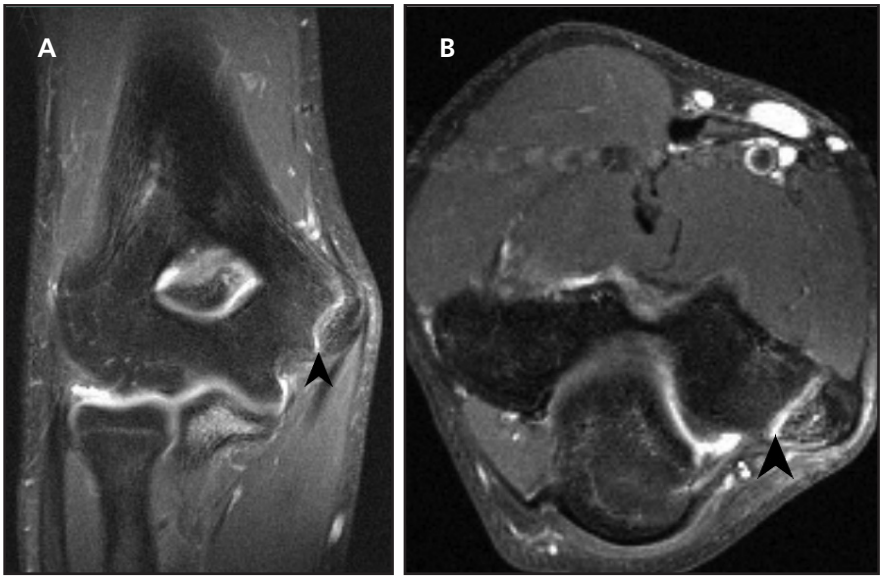


FIGURE 4. *Little Leaguer's elbow. Coronal fluid-sensitive MR image (A) demonstrating reactive marrow edema and fluid-like signal along the medial epicondyle apophyseal margin (arrowhead). Axial fluid-sensitive MR image again demonstrating marrow edema and medial epicondyle apophyseal edema (arrowhead).*

the adult, repeated valgus stress results in degeneration and tearing of the ulnar collateral ligament. In the adolescent, the medial epicondyle apophysis is at increased risk of injury because it is intrinsically weaker than the ulnar collateral ligament.[2] Apophysitis can be attributed to high pitch counts, and throwing off-speed and breaking pitches can accentuate the valgus stress. Clinical presentation includes pain and tenderness at the medial elbow, weakness and limited range of motion.

MRI will reveal apophyseal and subjacent bone marrow edema (**Figure 4**).[4] The ulnar collateral ligament should also be evaluated for sprain, which will manifest in thickening and increased intrasubstance signal on T2-weighted sequences.[5] High-grade partial and complete ligament tears are less likely in this population but should be excluded. Greater than 3-5 mm of physeal widening is an indication for surgical fixation due to risk of nonunion.[5]

In addition to medial tensile injury, concomitant lateral compressive injuries that may be identified include osteochondral lesion of the capitellum (see section below) and Panner disease. Panner disease is a self-limiting osteochondrosis involving the entire capitellum and is thought to result from vascular interruption secondary to compression.[2] It has been described on MRI as paraphyseal marrow edema in the absence of an osseous or chondral defect.[5] A late MRI manifestation of Panner disease is the replacement of normal fatty marrow signal with patchy sclerosis on T1WI.[4]

Physeal Stress Injuries

The physis, or "growth-plate," is characterized by a radiolucent line on x-ray between the epiphysis and metaphysis in the skeletally immature patient. The physis eventually disappears as endochondral ossification is completed, leaving a physeal scar. Like the apophysis, the physis is subject to stress during repetitive motion. Stress at the physis is due to compressive force, in contrast to the traction force exerted upon the apophysis. The peak incidence of physeal stress injury occurs between ages 11 and 14 years.[6]

Common locations for physeal stress injuries include the wrist, knee and shoulder. Clinical presentation includes pain, swelling and weakness. If left untreated, physeal stress injuries

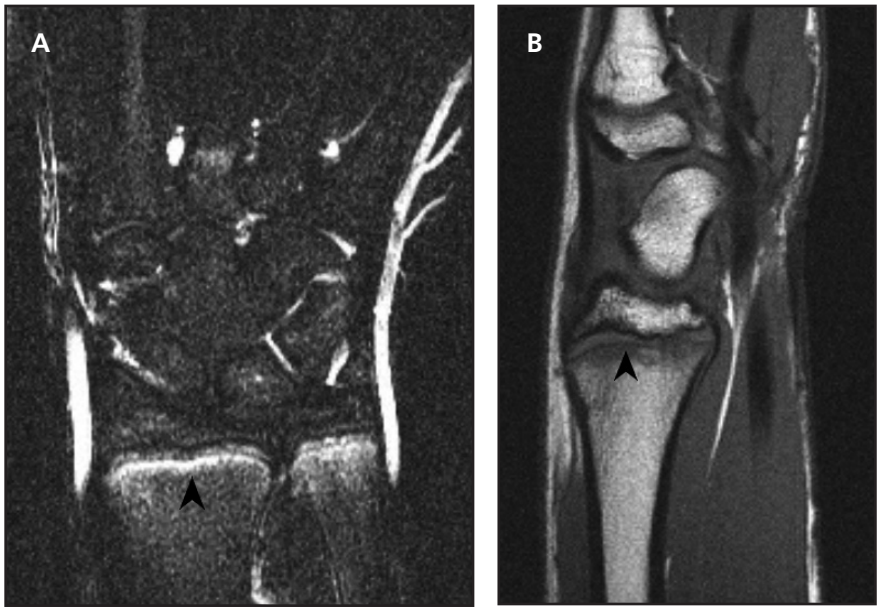


FIGURE 5. *Gymnast wrist. Coronal fluid-sensitive MR image (A) demonstrating physeal widening and edema-like signal (arrowhead). Sagittal PD MR image (B) demonstrating widening and irregularity of the physis (arrowhead).*



FIGURE 6. *Tibial stress fracture. Coronal T1-weighted MR image (A) demonstrating horizontally oriented linear hypointense signal at the proximal tibia corresponding to a stress fracture line (white arrowhead) with surrounding ill-defined hypointense marrow signal. Coronal fluid-sensitive MR image (B) demonstrating marrow edema with central linear hypointense signal corresponding with a stress fracture line (arrowhead).*

can result in growth cessation, length discrepancy, angular deformity and even lifelong disability. The mainstay of treatment is limitation and modification of activity. Diagnosis can be made radiographically with signs including soft-tissue swelling, osseous irregularity and widening of the physis. MRI will reveal physeal irregularity, widening, paraphyseal marrow edema and osseous or fibrous physeal bridging.[6]

Radial Physeal Stress Syndrome: Gymnast Wrist

A common physeal stress injury seen in adolescent gymnasts is gymnast wrist, with a significantly higher prevalence among females. Gymnastics often involve inverted maneuvers resulting in supraphysiologic compressive force at the wrist. Repeated axial loading of the wrist causes injury to the physis leading to premature closure. MRI will reveal physeal widening, which is more pronounced at the volar aspect owing to repetitive hyperextension at the wrist (**Figure 5**).[4] A physeal bar or osseous bridge can develop in some instances further altering development. Long-standing stress injury may manifest in positive ulnar variance and Madelung deformity. Positive ulnar variance can lead to ulnar impaction syndrome causing stress on the triangular fibrocartilage complex (TFCC) and lunate.[4] Accordingly, MRI may reveal TFCC and/or lunotriquetral ligament tears and degenerative cystic change along the ulnar aspect of the proximal lunate.

Stress Fracture

Stress fractures are characterized by abnormal stress on normal bone and often occur at the metaphyseal-diaphyseal interface. The most common locations for stress fractures occur in the weight-bearing lower extremities, specifically the tibia, tarsal navicular, metatarsal and fibula.[7] Clinical presentation includes pain, tenderness, and swelling aggravated by weight-bearing activities. Stress fractures can be subtle to imperceptible on radiographs depending on acuity. MRI is the most sensitive modality and will reveal periosteal and/or marrow edema. Linear, hypointense signal on T1WI corresponding to the fracture line is seen in higher-grade stress fractures.[7]

Tibial Stress Injury

Medial tibial stress syndrome, or "shin splints," results in diffuse medial tibial pain and is caused by local inflammation due to activity.[8] The Fredericson Classification System serves to grade medial tibial stress injuries based on MRI characteristics and thereby assist in management.[7] A high-grade medial tibial stress injury displays a

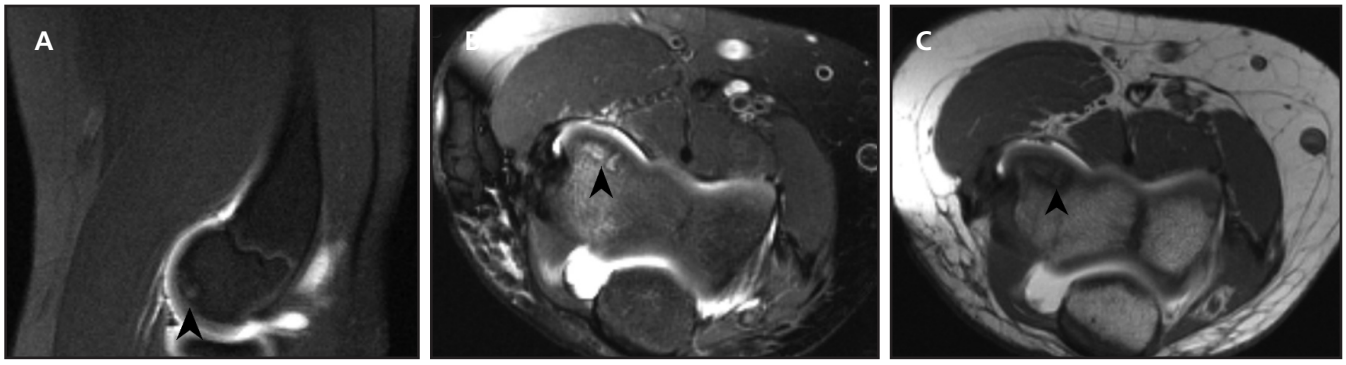


FIGURE 7. *Capitellum OCD. Sagittal T1 fat-saturated arthrogram MR image (A) demonstrating abnormal subchondral signal at the capitellum of the humerus (arrowhead). Axial fluid-sensitive MR image (B) demonstrating a subchondral defect with surrounding marrow edema (arrowhead). There is no associated cartilaginous discontinuity or high-signal rim. Axial T1-weighted MR image (C) further delineates the osteochondral fragment at the capitellum of the humerus (arrowhead).*

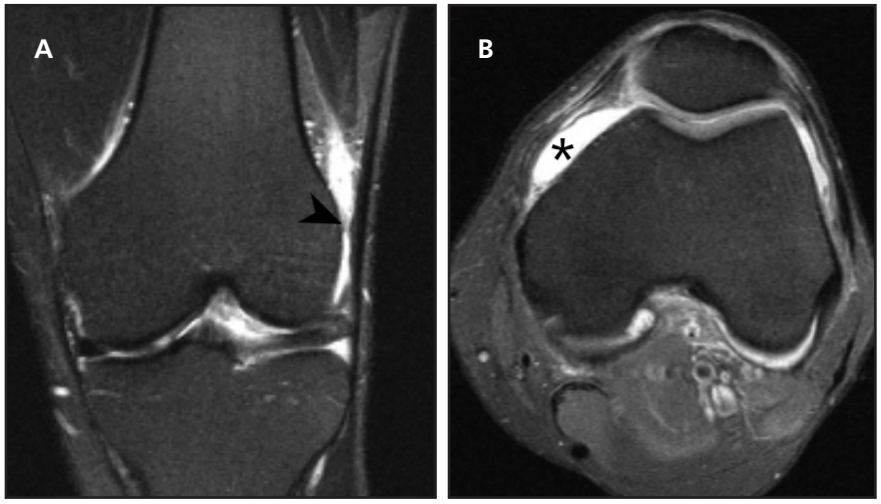


FIGURE 8. *Iliotibial band friction syndrome and pitfall. Coronal fluid-sensitive MR (A) demonstrates the soft-tissue T2-hyperintense signal (arrowhead) interposed between the distal iliotibial band and the lateral femoral condyle. A common pitfall is displayed in another patient (B) with an axial fluid-sensitive MR image displaying normal joint fluid extending into the lateral synovial recess (asterisk). This recess should not be confused with soft-tissue edema or inflammation.*

hypointense linear intracortical fracture line with surrounding hyperintense marrow signal on fluid-sensitive sequences (**Figure 6**). This injury results from repetitive high-impact activity and these fractures may be complete or incomplete. Fractures occurring at the anterior aspect of the tibia typically result from jumping-type stress whereas posterior fractures typically result from running-type stress. There is a higher incidence of tibial stress fracture in female adolescent athletes and those with pes cavus deformity. Patients tend to report a deep, throbbing pain localized to the fracture site. In all cases of tibial stress injury, activity cessation is the first-line treatment.

Osteochondral Lesions

Osteochondral lesion/defect, or osteochondritis dessicans (OCD), is characterized by separation of the osteochondral body from the subchondral bone. Disruption of the articular cartilage can result in local tenderness and a locking sensation. The most common location for development of an osteochondral lesion is the medial femoral condyle. Other commonly implicated locations include the humeral head, talar dome, and capitellum of the humerus. When left undiagnosed, osteochondral lesions may progress to secondary osteoarthritis. Treatment depends on severity with unstable lesions requiring surgical intervention.

Circumferential hyperintense T2-signal along the nonarticular portion of the lesion indicates fragment instability.[4] Other MRI findings suggesting instability include numerous or large underlying cysts, fluid-filled osteochondral defect, and a T2-hyperintense osteochondral fracture line surrounding the defect. In severe cases, the lesion will be identified as a displaced, intra-articular loose body.

Osteochondritis Dessicans: Capitellum of the Humerus

Osteochondral lesions occurring in the capitellum of the humerus are a manifestation of lateral elbow compression. These lesions are frequently encountered in overhead throwing athletes and gymnasts. Osteochondral lesions are located at the anterolateral aspect of the ossifying capitellar epiphysis and occur when ossification is nearing completion. Patients will present with pain and swelling at the lateral elbow and a locking sensation. In contrast to Panner disease, imaging will reveal flattening of the articular surface.

Because of their anterior location, osteochondral lesions are best seen on sagittal and coronal MR images. Early MR findings include crescentic low signal at the subchondral capitellar surface on T1WI. Longstanding injury will demonstrate marrow edema and articular surface cartilage irregularity (**Figure 7**).[4] The joint space should be evaluated for intra-articular loose bodies. Pseudodefect of the capitellum presents as focal flattening of the posterior

capitellum with normal overlying articular surface cartilage.[4] A pseudodefect of the capitellum should not be mistaken for an osteochondral lesion.

Friction Syndromes

Repetitive compression of soft tissues by bone or musculature can lead to inflammation and damage. Friction syndromes are more common in the adult, but have been described in the adolescent athlete population. Common areas for friction syndromes include the iliotibial band and patellar tendon-lateral femoral condyle.[9] MRI is helpful in diagnosing friction syndromes and identifying potential causes.

Iliotibial Band Friction Syndrome

Anatomically, the distal iliotibial band closely approximates the lateral femoral condyle as it inserts on Gerdy's tubercle at the lateral proximal tibia. With knee flexion and extension, the iliotibial band slides across the lateral femoral condyle surface. Friction is generated with activities such as running or cycling, which causes inflammation and pain at the lateral knee. MRI will reveal soft-tissue, edema-like signal interposed between the distal iliotibial band and lateral femoral condyle.[9] Of note, the lateral synovial recess of the anterior knee should not be confused with soft-tissue edema. In contrast to edema from iliotibial friction, this fluid-filled recess will not extend posterior to the lateral condyle (**Figure 8**).

Conclusion

Increasing incidence of sports-related overuse injuries is associated with early adolescent athletic specialization and high-intensity training.[1] More than ever, MRI is being utilized to effectively and safely identify overuse patterns of injury to expedite care and avoid potentially devastating complications. Treatment is usually conservative with an emphasis on activity cessation and/or modification, pain relief and rehabilitation. Radiologists should be familiar with the clinical presentation and common MRI findings of overuse injuries in adolescent athletes.

References

1. Lord J, Winell JJ. Overuse injuries in pediatric athletes. Curr Opin Pediat 2004;16:47-50.
2. Frush TJ, Lindenfeld TN. Peri-epiphyseal and overuse injuries in adolescent athletes. Sports Health 2009;1(3):201-211.
3. Kirkland WD. Imaging of the hamstrings. Semin Musculoskel Radiol 2008;12(1):028-041.
4. Delgado J, Jaramillo D, Chauvin AN. Imaging the injured pediatric athlete: upper extremity. RadioGraphics 2016;(36)6:1672-1687.
5. Wenzke DR. MR Imaging of the elbow in the injured athlete. Radiol Clin North Am 2013;51(2):195-213.
6. Jawetz ST, Shah PH, Potter HG. Imaging of physeal injury: overuse. Sports Health 2015;7(2):142-153.
7. Kijowski R, Choi J, Shinki K, Munoz Del Rio A, De Smet A. Validation of MRI classification system for tibial stress injuries. Am J Roentgenol 2012;198(4):878-884.
8. Franklyn M, Oakes B. Aetiology and mechanisms of injury in medial tibial stress syndrome: current and future developments. World J Orthop 2015;6(8):577-589.
9. Aydıngöz Ü, Özdemir ZM, GüneşA, Ergen FB. MRI of lower extremity impingement and friction syndromes in children. Diagn Interv Radiol 2016;22(6):566-573.

Decoding the Diffusion: Overview of Restricted Diffusion on Brain MRI

Jeremy Daniel, D.O., Yoon Cho, D.O., Donald von Borstel, D.O., Kyle Summers, D.O.

Department of Radiology, Oklahoma State University Center for Health Sciences, Tulsa, OK

Diffusion-weighted MR imaging (DWI) is a technique used to assess the random Brownian motion of water molecules within a certain voxel of tissue. In other words, DWI is used to determine the ease of molecular diffusivity of water within a tissue. Many pathologies cause restricted extracellular diffusion of water protons including infarction, cytotoxic edema, high cellularity within tissue, viscous fluid, demyelination, and metabolic disturbances. Restricted diffusion is seen as high-signal intensity on DWI with corresponding reduced apparent diffusion coefficient (ADC) values. ADC is a measurement of the diffusion of water molecules in a given tissue. ADC values are measured in units of 10^{-6} mm^2/s with ranges of reference values known for specific tissues within the brain. DWI is expressed with a b-value that is dependent on the characteristics of a sequence. The b-value will rise with increased diffusion weighting of the sequence, with a b-value of 1000 s/mm^2 being sufficient enough to provide diagnostic value.[1] Not all hyperintense regions on DWI images are due to restricted diffusion. Areas of hyperintensity on T2-weighted imaging (T2WI) may also be seen on diffusion imaging because DWI is intrinsically T2-weighted. This process is referred to as "T2 shine-through," and can be mitigated with higher b values.[2] The most common use of DWI is in the setting of acute ischemia by determining the presence of restricted diffusion from cytotoxic edema secondary to cell death. We will discuss other central nervous system (CNS) abnormalities where restricted diffusion plays an important diagnostic role in determining the underlying etiology of a CNS abnormality.

Vascular Etiologies

Ischemia-infarction

Stroke is a major cause of morbidity and mortality throughout the world with more than 795 000 cases occurring in the US each year. Approximately 80% of these events occur secondary to an acute ischemic event, often due to arterial thrombosis.[3] Neurons lack the ability to store energy; therefore, brain tissue is hypersensitive to ischemia. In the absence of oxygen, a neuron can only maintain viability for 2 to 3 minutes.[3] Acute ischemia often presents with an irreversible central core infarct and surrounding hypoperfused tissue described as the penumbra. Increased intracellular water accumulation and decreased rate of molecular water diffusion occur within the injured tissue. Therefore, the earliest findings of ischemic stroke are restricted diffusion on DWI, and corresponding low ADC values typically seen in the vascular distribution of the occluded vessel. Corresponding reduced signal on ADC maps separates stroke from T2 shine-through (**Figure 1**).[4] These findings have been found to occur as early as 30 minutes after onset of ischemia with a sensitivity of 88% to 100% and specificity of 86% to 100%.[3] In contrast, CT and conventional MRI have < 50% sensitivities within the first 6 hours after the event.[3]

Hypoxic-ischemic Injury

Hypoxic ischemic brain injury commonly occurs in the setting of profound hypotension, reduced blood oxygenation, and cerebral hypoperfusion. Common causes in adults include postcardiac arrest, shock and drug overdose. Additionally, this can be seen in neonates due to perinatal asphyxia.[5] Imaging patterns are variable and depend on duration and severity of the hypoxic events. Mild to moderate global injury leads to watershed infarcts, which manifest on MRI as cerebral cortical and subcortical white matter T2 hyperintensity with restricted

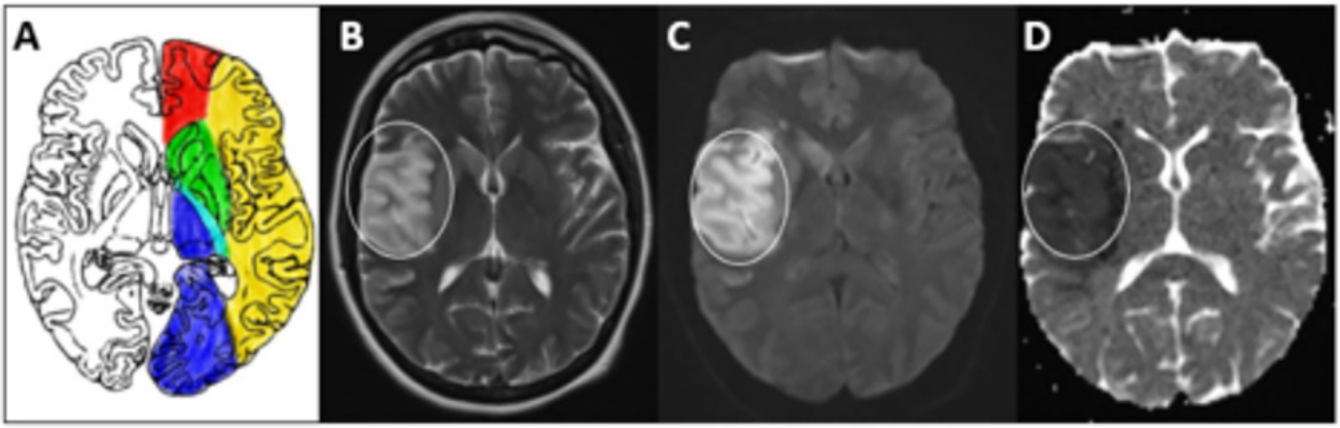


FIGURE 1. *Right MCA ischemic infarction. (A) Color-coded brain vascular territories — Red: Anterior cerebral artery, Green: Lenticulo-striate arteries, Yellow: Middle cerebral artery, Light blue: Anterior choroidal artery, and Blue: Posterior cerebral artery. Axial T2WI (B) demonstrating hyperintense signal (white circles) involving the right MCA territory with hyperintensity on DWI (C) and corresponding reduced signal on ADC map (D).*
**All illustrations original with credit: Dr. Yoon Cho*

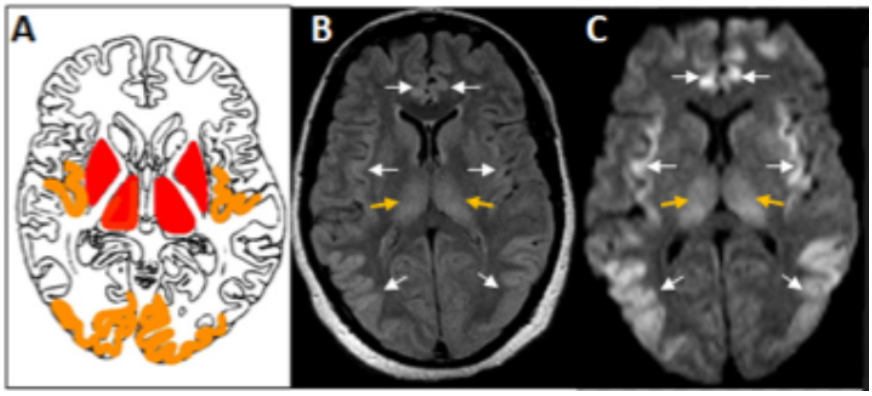


FIGURE 2. *Hypoxic ischemic injury. (A) Commonly involved areas of the brain: basal ganglia and thalami (red) and the cerebral cortex of temporal and occipital lobes (orange). Axial T2WI image (B) demonstrating hyperintense signal involving the bilateral cingulate gyri, insula, and occipital cortex (white arrows) and the bilateral thalami (orange arrows) with corresponding increased signal on DWI (C).*

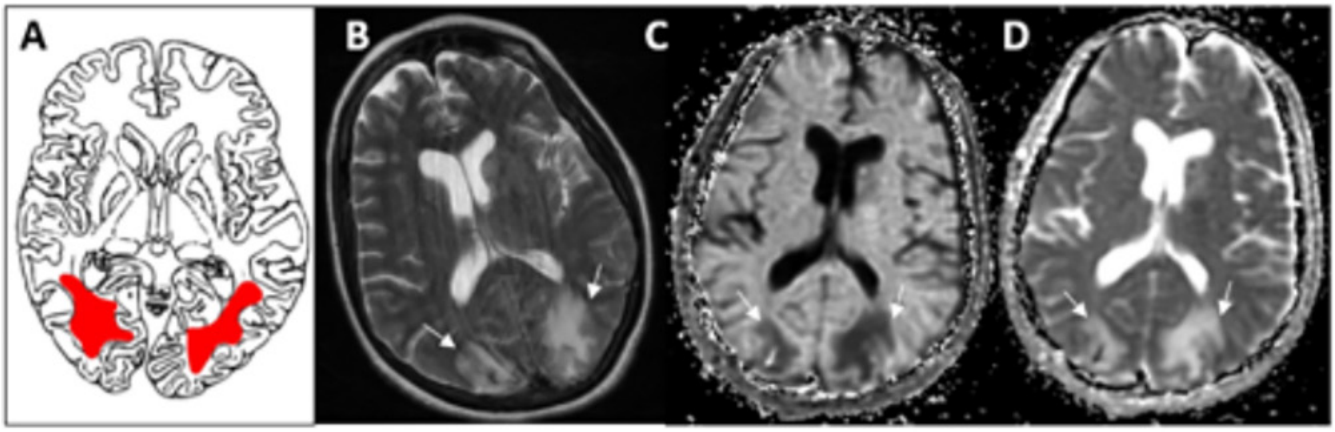


FIGURE 3. *Acute hypertensive encephalopathy (PRES). (A) Commonly involved areas of the brain: subcortical white matter of the occipital lobes (red). Axial T2-weighted (B) demonstrating hyperintense signal involving the bilateral subcortical occipital white matter (white arrows) with reduced signal on the exponential ADC image (C) and corresponding increased signal on the DWI (D) image secondary to vasogenic edema.*

diffusion between major arterial territories (**Figure 2**).[6] In severe injuries, grey matter structures such as the basal ganglia, thalami, and hippocampi are affected first due to their high metabolic demand. DWI is the first sequence to show pathology, and can demonstrate hyperintensity in the affected areas within hours of the inciting event. Increased T2-signal can typically be seen after approximately 24 hours in the early subacute phase.[7] This is due to increased edema in the injured gray matter structures.

Acute Hypertensive Encephalopathy

Acute hypertensive encephalopathy, also known as posterior reversible encephalopathy syndrome (PRES), is a neurotoxic state that is most likely due to an inability of the posterior circulation to autoregulate in response

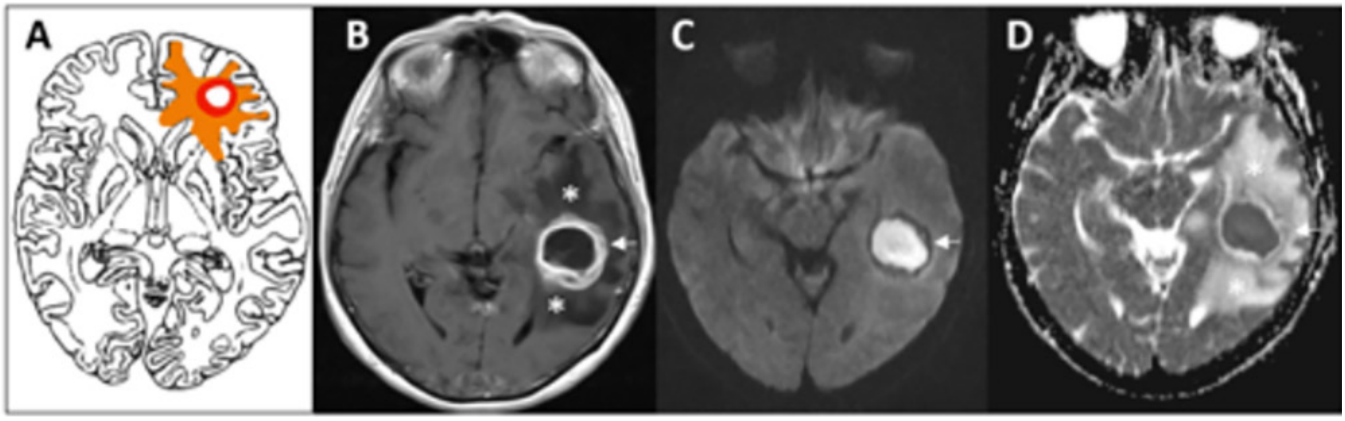


FIGURE 4. *Abscess. (A) Commonly involved areas of the brain: Typically involves subcortical white matter and can present as ring-enhancing lesions (red) with extensive T2-hyperintense vasogenic edema (orange). Axial T1 postcontrast image (B) demonstrating a left temporal ring-enhancing lesion (white arrow) with surrounding extensive vasogenic edema (asterisk) and internal restricted diffusion on DWI (C) with corresponding reduced signal on ADC map (D).*

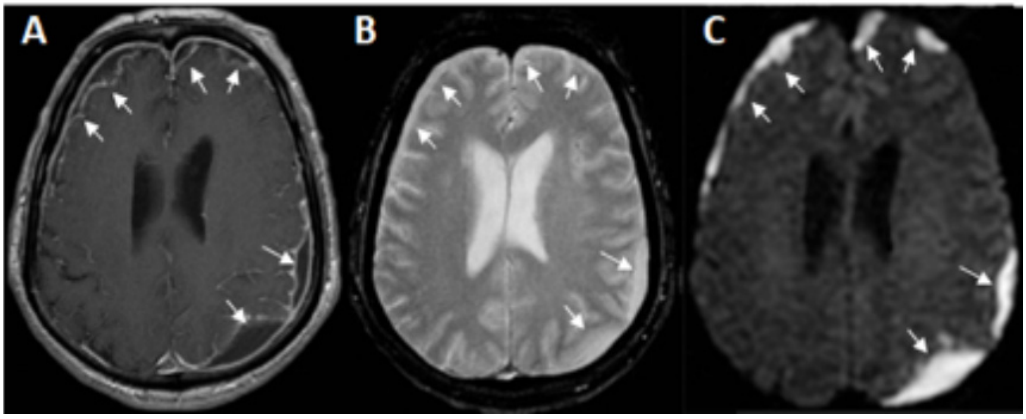


FIGURE 5*. Subdural empyema. Axial T1 postcontrast image (A) demonstrating multiple rim-enhancing subdural fluid collections along the cerebral convexities (white arrows) without susceptibility on GRE imaging, (B) which excludes subdural blood products. Hyperintense signal on DWI (C) is often the earliest imaging finding.*

to acute changes in blood pressure. It is most commonly associated with eclampsia and severe hypertension. PRES has also been associated with severe systemic infection, autoimmune disease, post-transplant patients on cyclophosphamide, and in patients undergoing high-dose chemotherapy.[8] Some of the many associated clinical symptoms include altered mentation, seizures, visual disturbances, and nausea. MR characteristics include T2-hyperintensity in the cortex and subcortical white matter of the occipital and parietal regions. Focal areas of restricted diffusion on DWI can be seen in up to 26% of cases (**Figure 3**).[8] Although PRES is predominantly composed of vasogenic edema that resolves over time, these focal areas of restricted diffusion are likely secondary to cytotoxic edema from cell death in more severe cases.

Venous Infarction

Venous infarction is a less common cause of stroke than its arterial counterpart. It is thought to occur most often in young women due to increased hypercoagulability when taking oral contraceptives and in pregnancy. However, more than 100 causes of venous thrombosis have been described, which occur secondary to direct involvement of the dural venous sinuses (trauma, infection), dehydration, endothelial damage, malignancy, or other underlying causes of hypercoagulability. Typical clinical presentation includes headache and focal neurologic deficits. Symptoms vary depending on thrombus location. The superior sagittal sinus is most commonly involved. Although less common, thrombosis will occur in the deep venous system approximately 16% of the time and the cortical veins approximately 17% of the time. On imaging, intracranial hemorrhage will occur approximately 30% to 40% of the time.[9] Therefore, concern for venous infarct should be raised in patients with lobar intracranial hemorrhage of unknown origin as well as cerebral infarction that crosses typical arterial boundaries. MR findings of venous thrombus are variable depending on the age of blood product. However, DWI sequences remain extremely helpful in determining the presence of acute infarction within the territory of venous thrombosis.[9]

Infectious Etiologies

Abscess

Cerebral pyogenic abscess is a serious condition usually occurring 10 to 14 days after the onset of underlying cerebral infection, referred to as cerebritis. Infection can be iatrogenic from sinonasal, skull base, or other intracranial procedures or spread hematogenously from

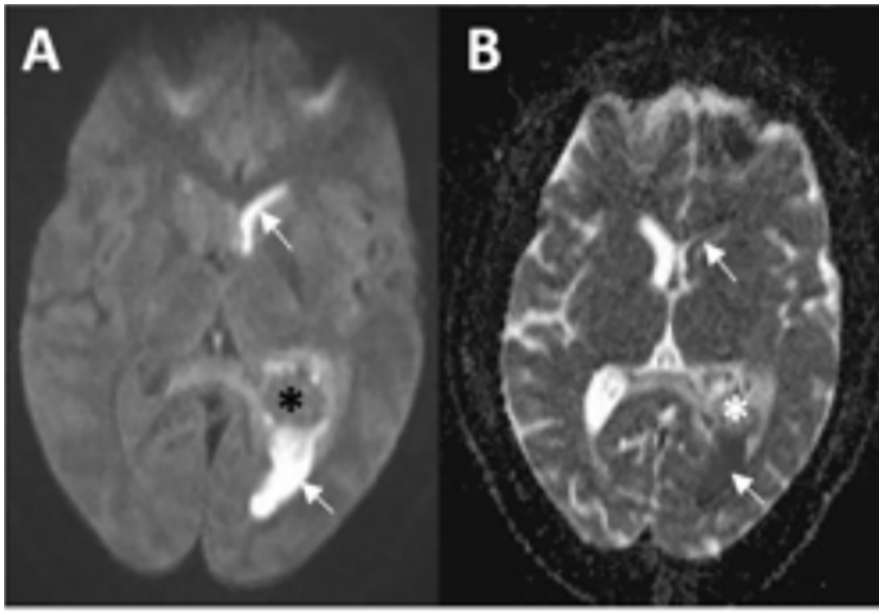


FIGURE 6. *Ventriculitis. Axial DWI (A) demonstrating hyperintense intraventricular signal (arrows) with left lateral intraventricular debris (asterisk) and corresponding low signal (arrows) on the ADC map (B).*

lung and sinonasal infections, systemic disease, dental abscess, and in the setting of infective endocarditis. The most common bacteria involved is *S. Pneumoniae*. The typical appearance of brain abscess on MRI is a ring-enhancing lesion that is T2-hyperintense with low or intermediate signal intensity on T1-weighted imaging (T1WI) (**Figure 4**). Central restricted diffusion is often present on DWI with corresponding low ADC values. Research suggests that DWI may be more sensitive than conventional MR when trying to distinguish a cystic mass from a brain abscess. This is because the purulence within a brain abscess is very hyperintense on DWI with corresponding low ADC values. Necrotic and cystic tumors have intermediate signal intensity on DWI with elevated ADC values.[10]

Empyema

Empyema is a life-threatening suppurative fluid collection in the epidural or subdural space, commonly due to bacterial meningitis, paranasal sinus disease, and otomastoiditis. Epidural empyemas often occur along the frontal convexities as a consequence of frontal sinusitis and erosion of the posterior wall of the frontal sinus, known as a "Pott's puffy tumor." Empyemas can also occur in the postsurgical or post-traumatic setting. Imaging features will demonstrate a rim-enhancing fluid collection within the subdural space. Lesions typically restrict diffusion. DWI sequences may be helpful in follow-up imaging of known infection with research showing that DWI sequences show changes earlier than contrast-enhanced T1WI (**Figure 5**).[11] Chronic subdural hematoma may be difficult to differentiate from empyema, and T2*-weighted sequences such as gradient echo or susceptibility-weighted imaging can differentiate these entities.

Ventriculitis

Ventriculitis is a ventricular ependymal infection typically occurring in the setting of meningitis, ruptured cerebral pyogenic abscess, a complication of cranial surgery or trauma, or in the setting of indwelling ventricular catheters. Characteristic imaging findings on MR are ventriculomegaly with dependently layering intraventricular debris that restricts diffusion (**Figure 6**).[12]

Viral Encephalitis (Herpes, HIV, etc.)

Viral encephalitis can either be primary or secondary. In primary encephalitis, the virus directly involves the CNS. In secondary encephalitis, the virus spreads to the brain from another part of the body. Many viral pathogens can affect the CNS, although the most common cause of fatal sporadic necrotizing encephalitis is *Herpes simplex* encephalitis. HSV encephalitis classically presents as T2-hyperintensity with variable gyriform enhancement and restricted diffusion in bilateral mesial temporal lobes (**Figure 7**).[13]

Progressive Multifocal Leukoencephalopathy

Progressive multifocal leukoencephalopathy (PML) is a subacute opportunistic infection caused by reactivation of *JC virus* in the oligodendrocytes of immunocompromised patients, resulting in areas of demyelination. Imaging findings include asymmetric, predominantly subcortical, T2-hyperintensities that involve the u-fibers and lack mass effect or enhancement (**Figure 8**).[13] PML lesions can demonstrate scattered areas of restricted diffusion at their periphery, which is thought to correlate with areas of lesion expansion.[14]

Creutzfeldt-Jakob Disease

Creutzfeldt-Jakob disease (CJD) is a rapidly progressing CNS prion disease resulting in dementia and death usually occurring within the first year of symptom onset. CJD is transmitted by exposure to brain or nerve tissues via "prion" – a misfolded functional nucleic acid protein. Most cases happen sporadically. Patients undergoing transplantation or hormonal therapy are also at risk. Clinical symptoms of those exposed to CJD include rapidly progressing dementia, ataxia, or generalized myoclonus. Imaging findings demonstrate increased T2 signal and restricted diffusion in the supratentorial gray matter, cortex, and white matter. Increased signal in the dorsal thalamus ("pulvinar sign") and posterior thalamus ("hockey stick sign") are characteristic findings,[13] and increased DWI signal may be the first abnormality seen on MR in early cases of CJD (**Figure 9**).[15] There is no

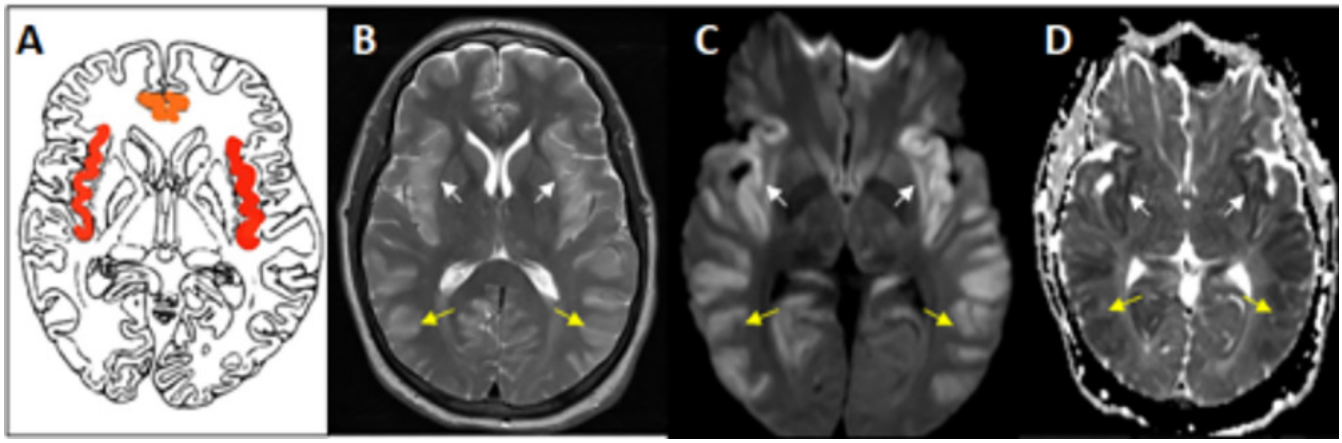


FIGURE 7. *Herpes encephalitis. (A) Commonly involved areas of the brain: gyriform enhancement of the bilateral mesial temporal lobes, insula, (red) and cingulate gyri (orange). Axial T2WI (B) demonstrating hyperintense gyriform signal involving bilateral insula (white arrows) and temporal lobes (yellow arrows) with hyperintensity on DWI (C) and corresponding reduced signal on ADC map (D).*

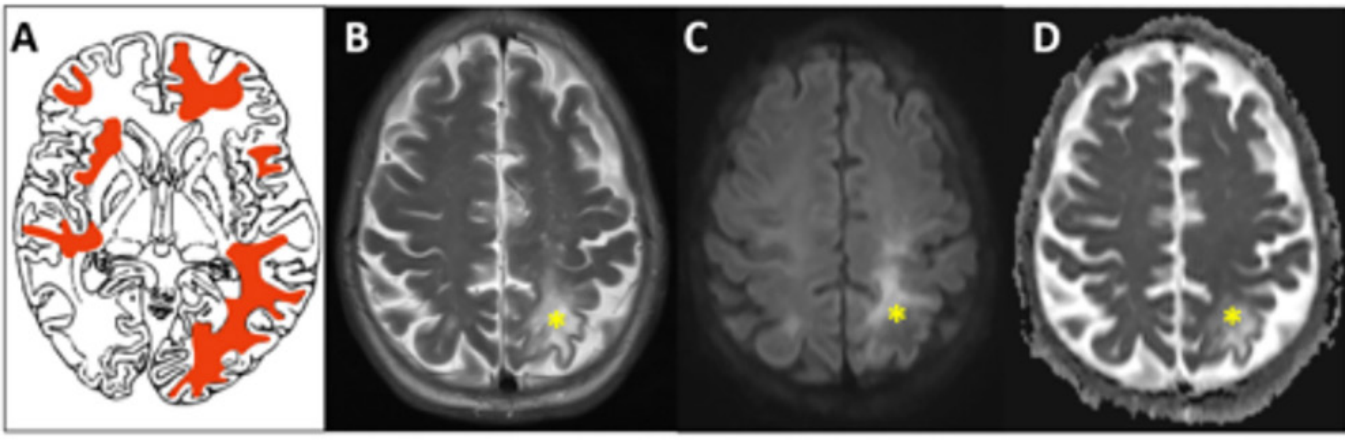


FIGURE 8. *Progressive multifocal leukoencephalopathy. (A) Commonly involved areas of the brain: predominantly subcortical white matter involving the u-fibers (red). Axial T2WI (B) demonstrating T2 hyperintense signal in the left superior parietal lobe including u-fibers (yellow asterisks) with restricted diffusion on DWI (C) and corresponding reduced signal on ADC map (D).*

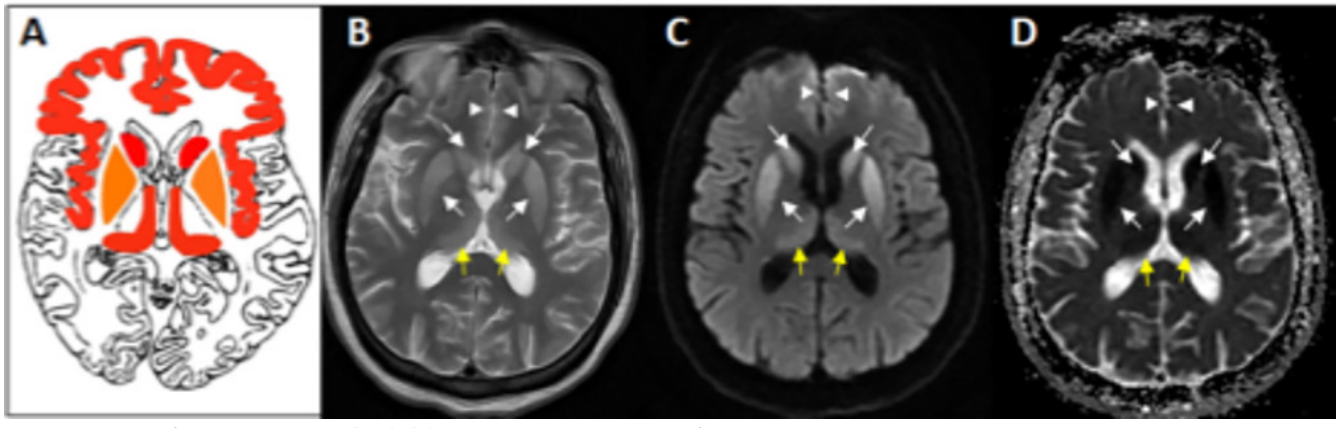


FIGURE 9. *Creutzfeldt-Jakob disease (CJD). (A) Commonly involved areas of the brain: supratentorial cerebral cortex, bilateral striata, and thalami (red and orange). Axial T2WI (B) demonstrating T2-hyperintense signal involving the bilateral striata (white arrows), thalami (yellow arrows), and anteromedial frontal cortices (arrowheads) with restricted diffusion on DWI (C) and corresponding reduced signal on ADC map (D).*

contrast enhancement or white matter involvement. Unfortunately, the prognosis is poor, with an 8.8-month survival rate.[15]

Toxoplasmosis

Toxoplasma gondii is a protozoan parasite that is known to infect the CNS in severely immunocompromised patients. Acute infection often occurs from reactivation of latent infections as 20% to 70% of all Americans are seropositive.[16] On MRI, lesions have a

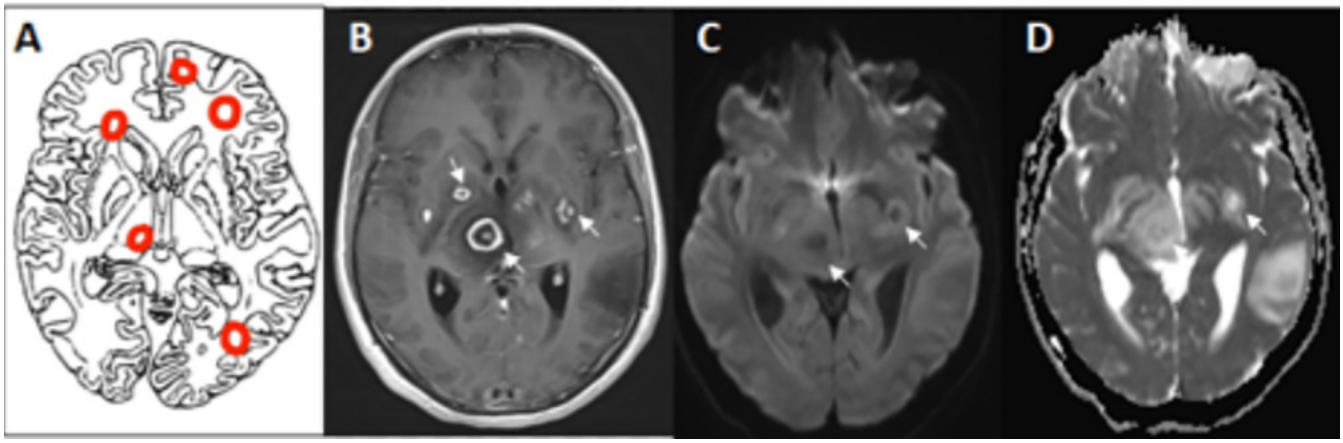


FIGURE 10. *Toxoplasmosis. (A) Commonly involved areas of the brain: Ring-enhancing lesions involving deep gray matter, periventricular white matter, and corticomedullary junctions (red circles). Axial T1 postcontrast image (B) demonstrating multiple ring-enhancing lesions in the basal ganglia (white arrows) with marginal ring-shaped restricted diffusion and surrounding vasogenic edema on DWI (C) and ADC maps (D).*

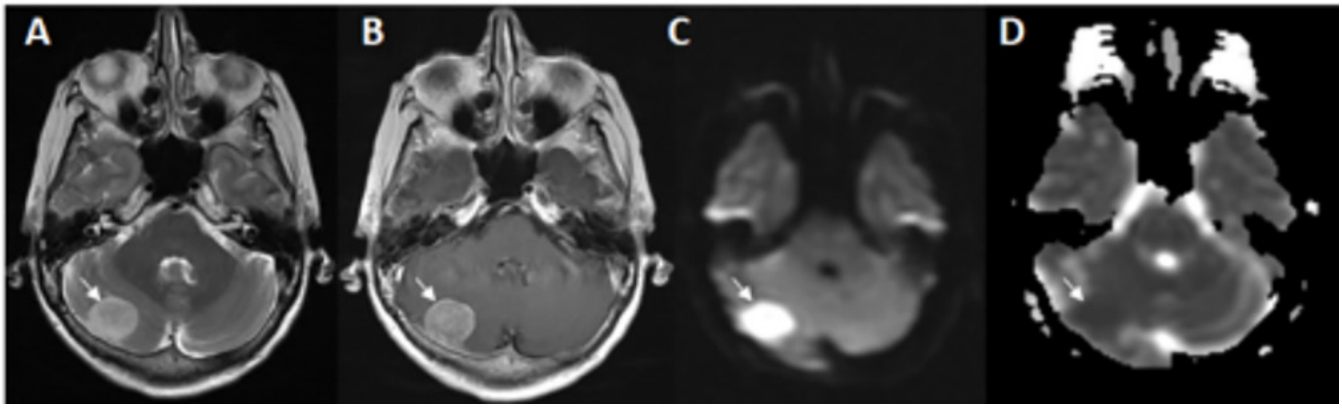


FIGURE 11. *Meningioma. Axial T2WI (A) and T1 postcontrast image (B) demonstrating a well-circumscribed extra-axial mass (white arrows) along the right posterior cerebellar convexity with increased signal on DWI (C) and corresponding decreased signal on ADC maps (D).*

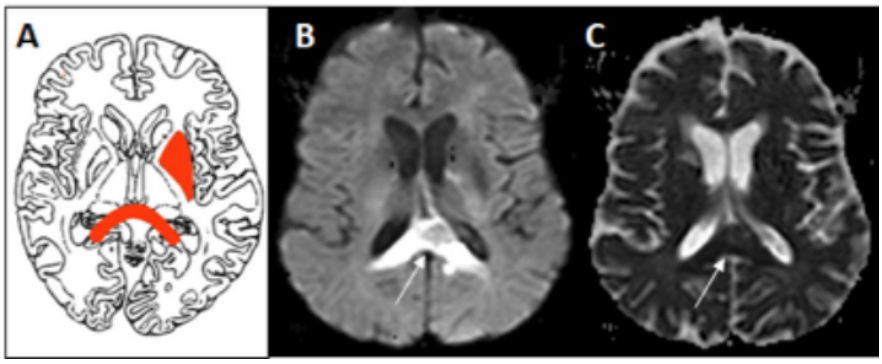


FIGURE 12. *CNS Lymphoma. (A) Commonly involved areas of the brain: Basal ganglia and corpus callosum (red). Axial DWI (B) demonstrates hyperintense signal of the corpus callosum (white arrow) and corresponding decreased signal on the ADC map (C).*

predilection for deep gray matter structures, periventricular white matter, and the corticomedullary junction. Large lesions can demonstrate rim enhancement, occasionally with a central dot creating the "target sign" (**Figure 10**).[13] On DWI sequences, these lesions may demonstrate mildly increased signal. However, ADC values are either the same or increased compared to surrounding white matter, which helps differentiate toxoplasmosis from cerebral abscess, which will demonstrate restricted diffusion with low ADC values.[17]

Neoplastic Etiologies

Meningioma

Meningioma is the most common extra-axial mass of the brain comprising 14% to 20% of all intracranial tumors.[18] Approximately 7.2% of meningiomas are atypical (WHO grade II) and 2.4% are malignant (WHO grade III).[18] Middle-aged women are most commonly affected, although meningioma is frequently seen in adults of all ages due to its high incidence. Ninety percent occur supratentorially with only 1 percent occurring outside the CNS. Meningiomas are iso- to hypointense on T1WI and iso- to hyperintense on T2WI. Avid homogenous enhancement is usually present after administrating gadolinium. DWI and ADC sequences demonstrate variable restricted diffusion (**Figure 11**). Views differ in the literature as to whether

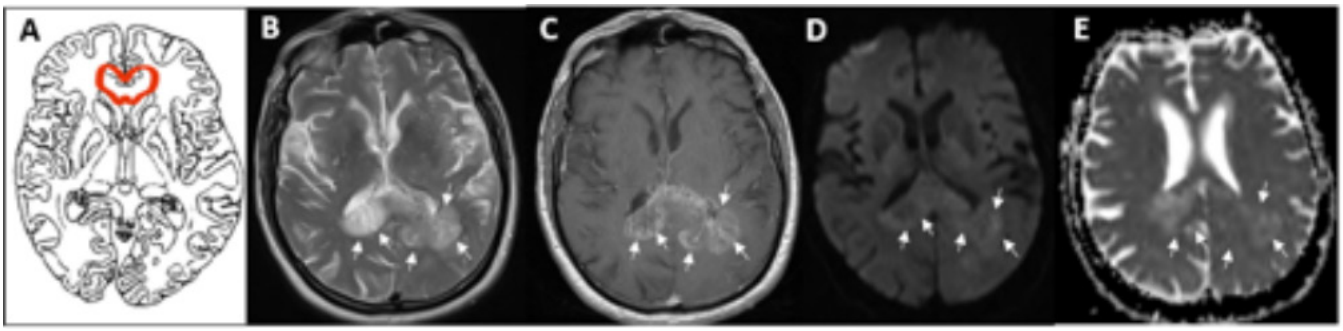


FIGURE 13. *Glioblastoma. (A) Commonly involved areas of the brain: cerebral hemispheres with extension across the corpus callosum, a classic "butterfly glioma" appearance (red circle). Axial T2WI (B) a large hyperintense mass with a heterogeneous rind of contrast enhancement on T1 postcontrast image (C) centered at the callosal splenium with involvement of the bilateral parietal and occipital lobes (outlined by white arrows) with increased signal on DWI (D) and corresponding slightly reduced signal on the ADC map (E).*

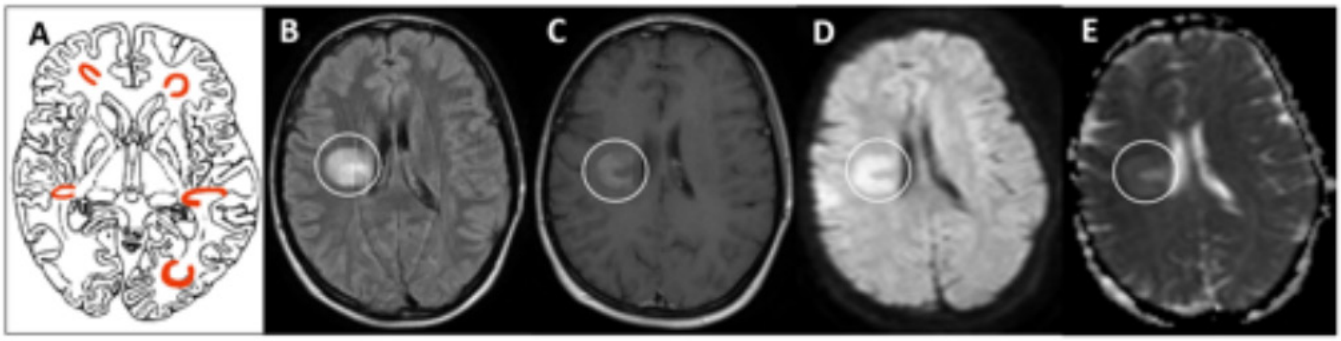


FIGURE 14. *Tumefactive multiple sclerosis. (A) Commonly involved areas of the brain: an incomplete ring-enhancing lesion involving periventricular white matter (red circle and red solid). Axial FLAIR image (B) demonstrating a mass (white circle) at the right centrum semiovale with incomplete ring enhancement on the T1 post-contrast image, (C) which demonstrates increased signal on DWI (D) and corresponding slightly reduced signal on ADC map (E).*

diagnostic ability can distinguish malignant and atypical subtypes from benign based on ADC values.[18,19]

Primary CNS Lymphoma

Primary CNS lymphoma (PCNSL) is most often seen in immunocompromised patients, particularly those with AIDS. It is believed that decreased function of suppressor T-cells in immunosuppressed patients is the underlying cause of PCNSL. Just as in other areas of the body, PCNSL can have a wide variety of appearances on imaging and can be difficult to differentiate from other entities such as CNS toxoplasmosis. Signal is variable on T2WI with most cases demonstrating homogenous enhancement after the administration of contrast. Restricted diffusion will be noted due to lymphoma's dense cellularity. It is important to note that corresponding ADC values will be lower than those in high-grade glial-based tumors such as GBM as well as metastasis (**Figure 12**).[20] Further studies have shown that ADC values may have importance in the response of PCNSL to chemotherapy with values increasing in response to successful treatment.[21]

Glioblastoma

Glioblastoma (GBM) is a WHO grade IV intracranial neoplasm and the most common astrocytoma. Glioblastoma is the most lethal glioma with only about a 10% survival rate at 2 years. Glioblastoma can occur anywhere in the cerebrum but frequently spares the occipital lobes. MR findings are characterized by the presence of necrosis. Findings include T1 hypo- to isointensity, T2 hyperintensity, and enhancement of solid components. Restricted diffusion is common and will be seen in the solid components (**Figure 13**). Lower ADC values correlate with higher-grade tumors and, therefore, can help differentiate astrocytomas.[22] The amount of T2-signal within the mass, degree of surrounding vasogenic edema, and postcontrast enhancement may have a direct relationship to long-term survival in patients with GBM.[23] Patients with typically more favorable outcomes are younger than 45 years and have wild-type tumor genetics with MGMT methylation.

Demyelinating Etiologies

Tumefactive Multiple Sclerosis

Multiple sclerosis (MS) is the most common demyelinating disease in the world and most commonly affects young females with peak age of 30 years. Demyelinating lesions in MS have a predilection for the supratentorial white matter, although infratentorial and spinal cord lesions are also common. Periventricular white matter lesions extending perpendicular to the lateral ventricles ("Dawson fingers"), callososeptal interface lesions, and juxtacortical white matter lesions are characteristic findings. Demyelinating lesions are best visualized on MRI with T2 and fluid-attenuated inversion recovery (FLAIR) sequences being the

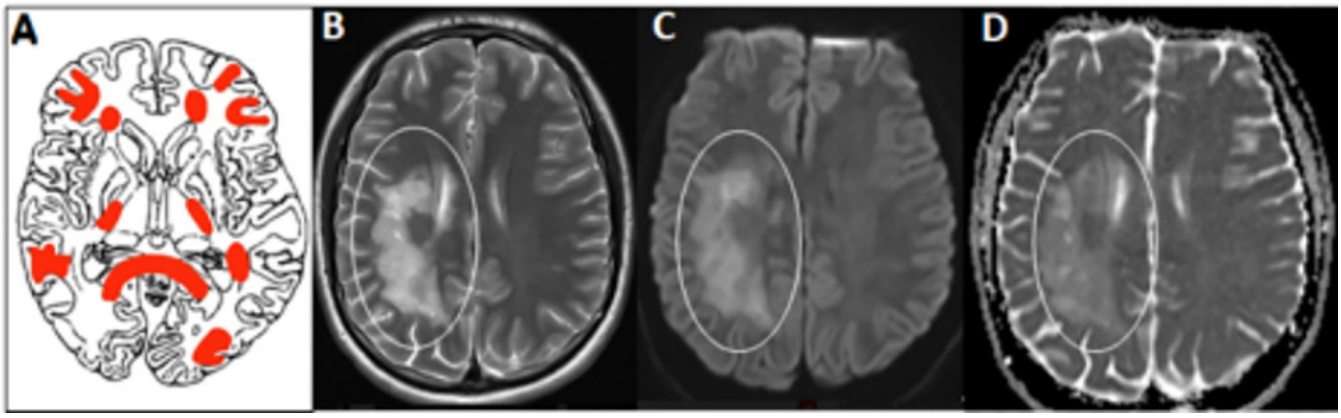


FIGURE 15. *Acute disseminated encephalomyelitis (ADEM). (A) Commonly involved areas of the brain: favors subcortical and deep white matter (red). Axial T2WI (B) demonstrating a T2-hyperintense signal (white circle) involving the right parietal lobe deep white matter with increased signal on DWI (C) and corresponding slightly reduced signal on ADC map (D).*

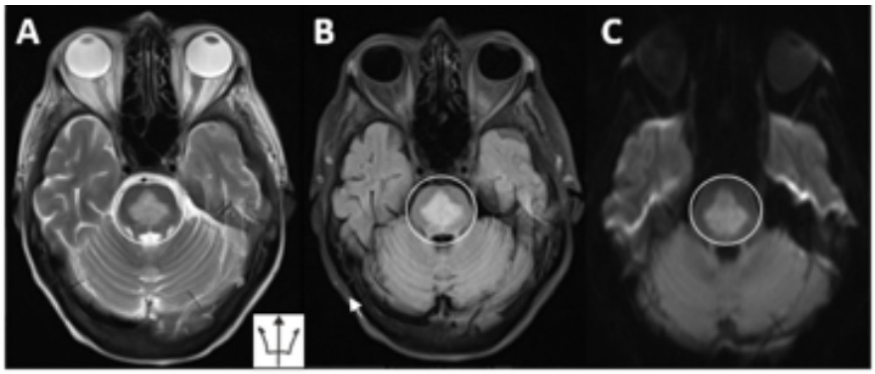


FIGURE 16. *Osmotic demyelination syndrome. Axial brain at the level of pons demonstrating a T2/FLAIR (A, B) hyperintense isolated pontine lesion (white circle) in "trident" shape with restricted diffusion on DWI (C).*

most sensitive. Radiologic diagnosis is possible when lesions are present in characteristic locations with dissemination in space and time (the modified McDonald criteria). There are multiple clinical subtypes and MS variants, and occasionally lesions can emerge in the form of large aggressive-appearing mass-like lesions. These lesions will have little surrounding edema and will not cause any significant mass effect when compared to aggressive tumors such as GBM.[24] Additionally, these lesions will demonstrate incomplete ring enhancement after contrast administration with the incomplete portion of the ring lying on the gray matter side of the lesion (**Figure 14**).[24] MS lesions are usually associated with increased diffusion. However, there are multiple reports of MS lesions with areas of restricted diffusion thought to be associated with active demyelination.[25]

Neuromyelitis Optica

Neuromyelitis optica (NMO) is a demyelinating disease caused by an autoantibody to the aquaporin 4 (AQP 4) water channel. Patients have variable clinical presentations, although this entity classically presents with bilateral optic neuritis and myelitis resulting in blindness and paraplegia. MR imaging of orbits may demonstrate edematous T2-hyperintense optic nerves, which enhance after administration of contrast. Traditionally, the brain is spared of demyelinating lesions. Lesions in the spine are characterized by longitudinal involvement of the cord for three or more contiguous vertebral segments. Lesions tend to involve the central gray matter along the central canal as this area corresponds to the most prominent expression of the AQP4 antigen.[26] Information is limited regarding the diffusion imaging in NMO. However, it is believed that optic neuritis in NMO may restrict diffusion while optic neuritis from other causes does not.[27]

Acute Disseminated Encephalomyelitis

Acute disseminated encephalomyelitis (ADEM) is mediated by antigen-antibody complexes and usually occurs in children in the postviral setting, although it can also present after vaccinations, in exanthematous disease of childhood, or be idiopathic. ADEM has no gender predilection as with other demyelinating diseases. The underlying etiology is thought to be secondary to an allergic or cell-mediated immune cross-reaction with a viral protein. Symptoms present similar to acute MS. ADEM is usually a monophasic disease with most patients reaching full recovery. However, in the acute phase, mortality rate is approximately 10% to 20%.[28] On MRI, multiple bilateral and usually asymmetric T2-hyperintense lesions will be present (**Figure 15**). In contrast to MS, ADEM favors subcortical and deep white matter regions without "Dawson's fingers" or involvement of the callosal-septal interface. Lesions are typically larger than those in MS and can involve the brain and spine as well as white and gray matter. Involvement of the deep gray matter nuclei, thalamus, and brainstem is common with subcortical and u-fiber involvement occurring frequently. Lesions may demonstrate peripheral rim enhancement or restricted

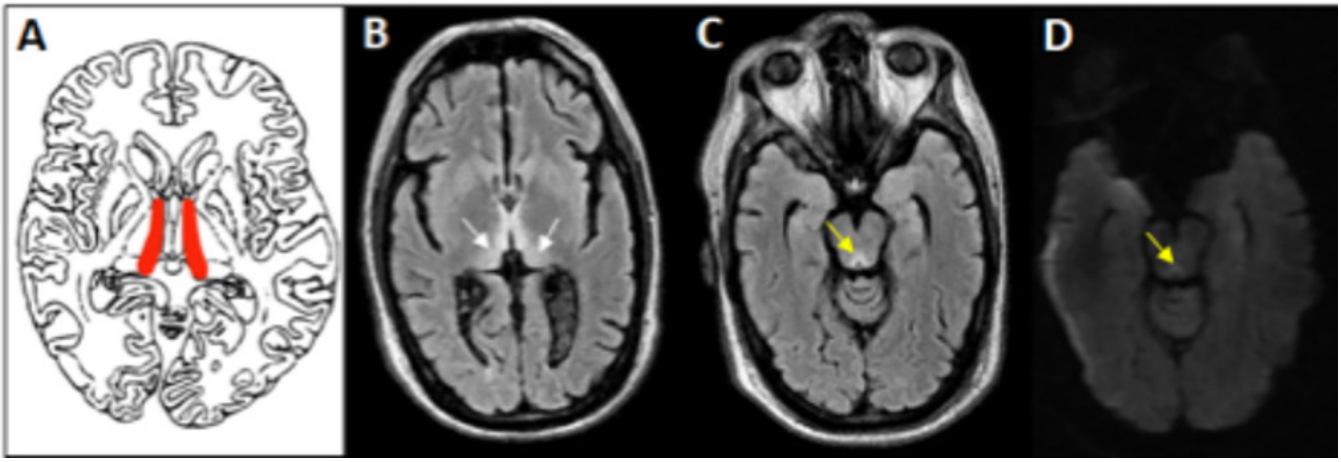


FIGURE 17. *Wernicke encephalopathy. (A) Commonly involved areas of the brain: bilateral periventricular thalami (red) and periaqueductal regions (not shown on drawing). Axial FLAIR image (B) demonstrating symmetric hyperintense signal involving the bilateral periventricular thalami (white arrows). Axial FLAIR image at the level of midbrain (C) demonstrates hyperintense signal along the periaqueductal region (yellow arrow) with subtle restricted diffusion on DWI (D).*

diffusion, likely secondary to the underlying active inflammatory process.[28]

Metabolic/Toxic Etiologies

Osmotic Demyelination Syndrome

Formerly known as central pontine myelinolysis (CPM), osmotic demyelination syndrome is a condition in which demyelination occurs secondary to rapid correction of electrolyte disturbances, most commonly hyponatremia. Oligodendroglial cells are particularly vulnerable to osmotic changes, and demyelination in this entity preferentially occurs in areas with higher concentrations of oligodendrocytes. Populations vulnerable to this condition include chronic alcoholics (60% to 70%), malnourished patients, chronically ill patients, patients with extensive burns, and transplant recipients.[29] The imaging findings include isolated pontine lesions (most common) or combined types (central and extrapontine areas) that demonstrate symmetric, trident-shaped, hyperintense signal abnormality on T2WI or FLAIR images (**Figure 16**).[30] Even before any signal abnormality is detected on T2WI or FLAIR images, restricted diffusion within the central pons may be identified within 24 hours of symptom onset.[31] Extrapontine demyelination can occur in the basal ganglia, thalami, peripheral cortex, and hippocampi. Hyperintense lesions in the caudate and putamen can precede central pontine lesions. The important distinction from other entities is that the lesions do not demonstrate enhancement.[30]

Hypoglycemic Encephalopathy

Hypoglycemic encephalopathy develops in insulin-dependent diabetic patients who present with blood glucose levels < 50 mg/dL. Clinical manifestation includes altered mental status, loss of consciousness or seizures. The earliest imaging finding is hyperintense signal on DWI and corresponding low ADC value (in the range of 448.82 ± 92.34 × 10^{-6} mm^2/s).[32] The most affected areas of the brain include the centrum semiovale, corona radiata, internal capsule, and splenium of the corpus callosum.[33] Relative sparing of the cerebellum and thalami are important distinctions from hypoxic ischemic injury. According to a study performed by Dr. Kang et al, patients with frontal and parietal cortical involvement had a worse clinical outcome compared to patients with only white matter involvement.[32]

Wernicke Encephalopathy

Wernicke encephalopathy is a devastating neurological disorder caused by vitamin B1 deficiency. This condition is often seen in the chronic alcoholic population, but also found in nonalcoholic populations with restricted diets.[34] Clinical manifestations include altered mental status (most common), oculomotor abnormalities, and ataxia. The earliest imaging finding of Wernicke encephalopathy is slightly increased signal on DWI of the bilateral periventricular thalami and periaqueductal regions. As this entity progresses, imaging findings include symmetric T2 and FLAIR hyperintense lesions affecting medial thalami (85%), the periaqueductal gray matter, mammillary bodies, tectal plate, and the periventricular gray matter anterior to the fourth ventricle (**Figure 17**). A 2009 study by Zuccoli et al states that contrast enhancement of the mamillary bodies and thalamus was the most specific finding among the alcoholic population.[35]

Carbon Monoxide Poisoning

Carbon monoxide (CO) is a colorless and odorless gas produced when fossil fuel is used for heating; thus, accidental CO poisoning is more prevalent in winter months. Carbon monoxide displaces oxygen from hemoglobin with higher affinity and causes hypoxia that can result in anoxic-ischemic encephalopathy. As previously discussed, the most vulnerable areas to hypoxic ischemic injury are the cerebral cortex with a predilection for the temporal lobes and hippocampi. Symmetric restricted diffusion of the globus pallidi is the most characteristic imaging finding of CO poisoning.[36]

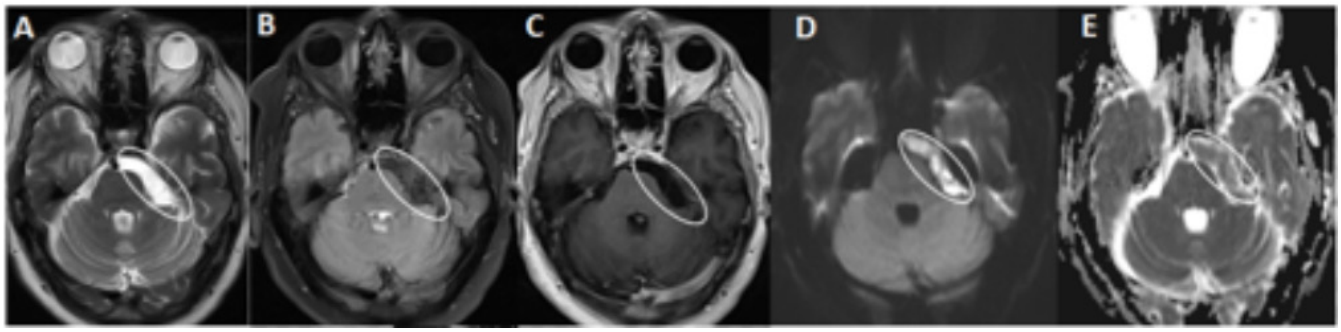


FIGURE 18. *Epidermoid cyst. There is an extra-axial mass (white ovoid circle) in the left cerebellopontine angle causing mass effect on the pons and demonstrating isointense to hyperintense to CSF on T1- (C) and T2-weighted/FLAIR (A/B) images. The mass demonstrates increased signal on DWI (D) and corresponding reduced signal on ADC (E).*

However, the first imaging finding during the acute phase of exposure to carbon monoxide is hyperintense signal on DWI affecting cerebral hemispheric white matter with associated signal loss on ADC. Relative ADC values are typically in the range of 180 x 10^{-6} mm^2/s.[37]

Ethylene Glycol and Methanol Toxicity

Ethylene glycol is used in polyester manufacturing and as the primary compound in antifreeze, which can also contain methanol. Accidental or intentional ingestion of ethylene glycol can cause neurotoxicity presenting with confusion and ataxia. Imaging findings include restricted diffusion involving the bilateral basal ganglia, thalami, amygdala, hippocampus, and cerebral cortices. DWI will demonstrate hyperintense signal involving the cerebral cortex.[38] Methanol toxicity presents with pallidal necrosis and optic nerve demyelination.[39]

Trauma

Diffuse Axonal Injury

When traumatic brain injury occurs, it can result in diffuse axonal injury (DAI) from rotational acceleration forces causing deformation of brain tissue and development of hemorrhagic or nonhemorrhagic traumatic lesions. Due to cellular swelling, or cytotoxic edema, FLAIR hyperintensity and restricted diffusion can be present in affected areas with low ADC values up to 18 days after the initial traumatic event.[40] The most commonly involved areas of the brain include the splenium of the corpus callosum, gray/white matter interface (especially involving the frontal and temporal lobes), and dorsolateral midbrain. Hemorrhagic lesions in DAI will present as hypointense foci on susceptibility-weighted images. The DWI signal abnormality will return to normal after 30 days.[41] In addition, in the setting of a high-velocity trauma, extremity long-bone fracture can occur and lead to propagation of bone marrow fat into the pulmonary vasculature. If a right-to-left cardiac shunt such as an atrial septal defect is present, fat emboli can travel to the CNS arterial vasculature and cause ischemic infarct, which can mimic the imaging pattern of diffuse axonal injury.[42]

Miscellaneous Etiologies

Epidermoid Cyst

Epidermoid cysts are benign intracranial congenital inclusion cysts that originate from ectodermal epithelial tissue from the pharyngeal pouch of Rathke during neural tube closure. The epidermoid cyst is lined by simple stratified cuboidal squamous epithelium and are isointense/hyperintense to cerebrospinal fluid (CSF) on T1WIs and T2WIs without internal contrast enhancement (**Figure 18**). The most useful distinction between epidermoid and arachnoid cyst is the restricted diffusion seen with epidermoid cysts.[43] The average ADC value of epidermoid cysts measures 1197 × 10^{-6} mm^2/s, which is approximately isointense to brain parenchyma.[44] The most common intracranial locations include the cerebellopontine angles (40% to 60%), suprasellar cistern, and fourth ventricle.[45] Epidermoid cysts are often treated with surgical excision if symptomatic.[44]

Choroid Plexus Cyst

Choroid plexus cysts, also known as xanthogranulomas, are common findings in utero between weeks 26 to 28 of gestation. Most choroid plexus cysts are 2 to 8 mm and often disappear on follow-up ultrasound screening.[46] Choroid plexus cysts are fluid-filled structures and follow CSF signal on T2WIs with iso- to hyperintense signal on T1WI due to proteinaceous content (**Figure 19**). If choroid plexus cysts persist and are > 1 cm, they are often associated with trisomy 18, trisomy 21, Klinefelter syndrome, and Aicardi syndrome.[46] On DWI, choroid plexus cysts demonstrate restricted diffusion with low ADC values.[47]

Status Epilepticus

Status epilepticus can locally increase cerebral metabolic activity and result in vascular hyperperfusion, which ultimately may lead to cerebral edema and decreased cerebral diffusion. The most common imaging findings include focal restricted diffusion with a cortical or subcortical distribution and corresponding T2/FLAIR hyperintensity with mild enhancement on postcontrast images.[48] According to Hubers et al, restricted diffusion is present at the seizure focus, the center of ictal activity with no clear location or laterality predilection.[49] However, earlier studies have discussed that the temporal lobe or hippocampal structures were believed to be the most prevalent sites of restricted diffusion.

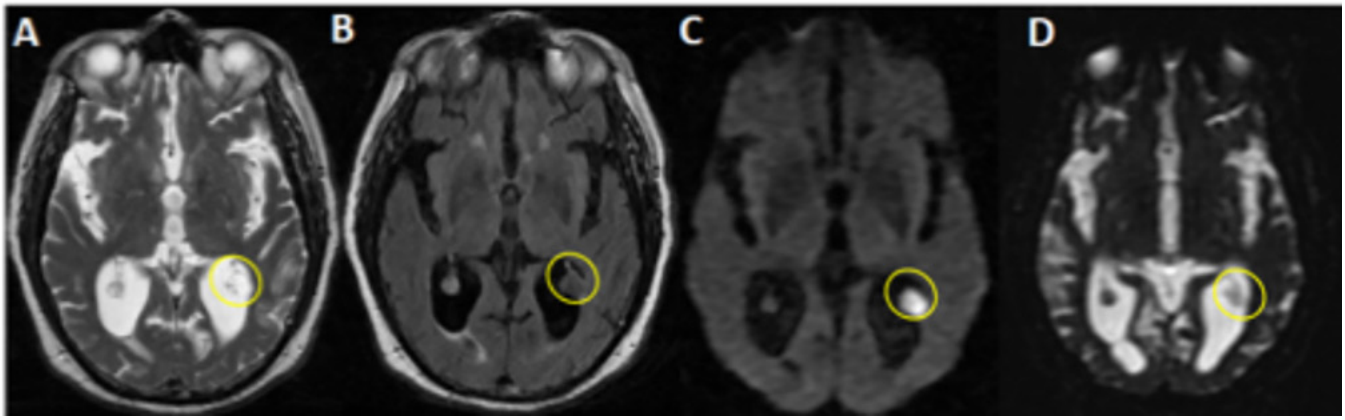


FIGURE 19. *Choroid plexus cyst. The left choroid plexus demonstrates a cystic lesion (yellow circle) that demonstrates signal that is isointense/hyperintense to CSF on T2-weighted/FLAIR (A/B) images. The lesion demonstrates increased signal on DWI (C) and corresponding reduced signal on ADC (D).*

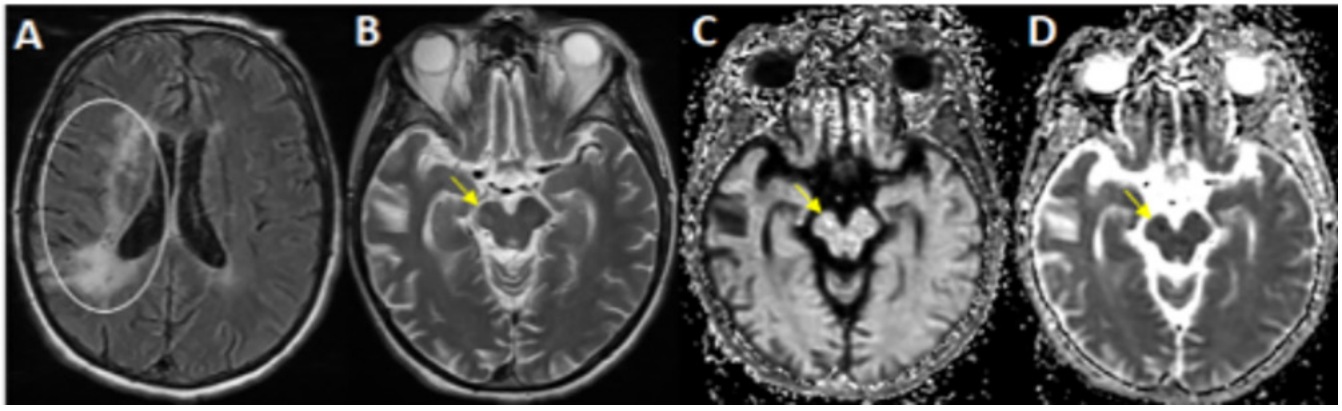


FIGURE 20. *Wallerian degeneration. Axial T2WI (A) demonstrates extensive encephalomalacia throughout the right MCA territory (white circle), consistent with chronic infarction. Asymmetry of the midbrain, right smaller than left, is consistent with Wallerian degeneration (yellow arrows) shown on T2 fat-saturated image (B), DWI (C), and ADC (D).*

Wallerian Degeneration

Wallerian degeneration refers to an anterograde degeneration of axons secondary to central neuronal injury and occurs in four distinct stages. In the first stage (within 4 weeks from the initial injury), myelin and axonal breakdown begins without visible signal abnormality on MRI. Later, there is myelin protein breakdown altering protein-lipid ratio in stage 2 (4 to 14 weeks) causing T2-hyperintense signal abnormality. Progression of gliosis and corresponding T2-signal abnormality occurs in stage 3 (14 weeks to months after the initial injury). Finally, stage 4 (years after the initial injury) shows atrophy of the involved corticospinal tract (**Figure 20**). Throughout the course of Wallerian degeneration, cytotoxic edema can be present leading to restricted diffusion of the involved white matter tract that can be seen as early as stage 1.[50] A study by DeVetten et al stated that early ADC signal decrease after acute stroke can predict early Wallerian degeneration and may increase a patient's clinical outcome by selecting patients for rehabilitation and neuroprotection trials.[51]

Conclusion

As we have seen, restricted diffusion patterns play an important role in the diagnosis of many CNS abnormalities. The ability to evaluate tissues on a cellular level gives us valuable knowledge of the underlying pathophysiologic processes within the CNS. Clinical medicine will benefit greatly as MRI continues to advance tissue characterization and more specific diagnoses. As such, the knowledge of typical restricted diffusion patterns of each CNS abnormality will assist radiologists in developing a succinct differential diagnosis guiding referring physicians to the correct diagnosis.

References

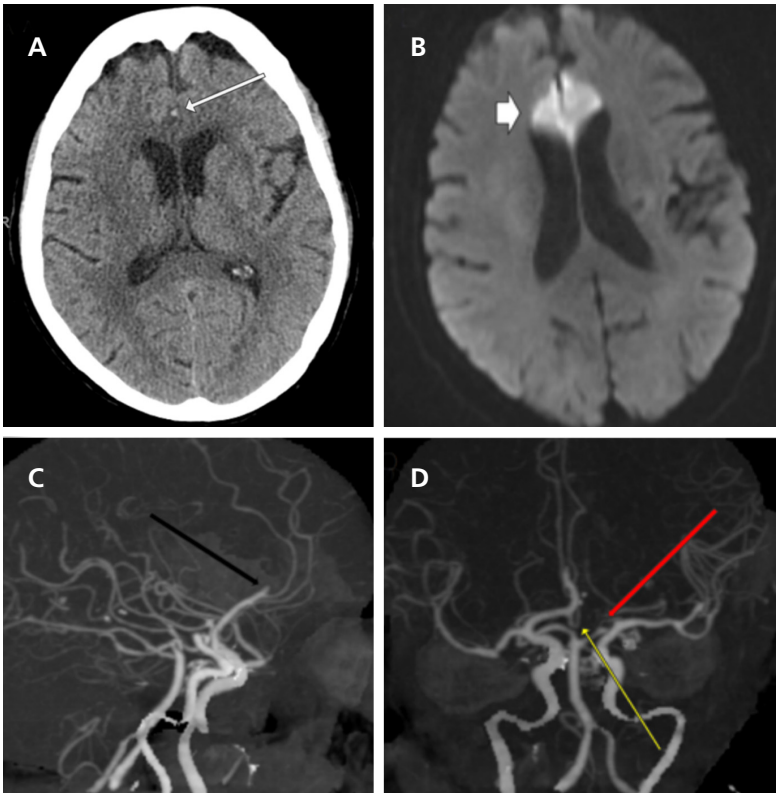
1. Helenius J, Soinne L, Perkiö J, et al. Diffusion-weighted MR imaging in normal human brains in various age groups. Am J Neuroradiol 2002;23(2):194-199.
2. Geijer B, Sundgren PC, Lindgren A, Brockstedt S, Ståhlberg F, Holtås S. The value of b required to avoid T2 shine-through from old lacunar infarcts in diffusion-weighted imaging. Neuroradiology 2001;43(7):511-517.
3. Srinivasan A, Goyal M, Al Azri F, Lum C. State-of-the-art imaging of acute stroke. RadioGraphics 2006;26(suppl 1):S75-95.
4. Allen LM, Hasso AN, Handwerker J, Farid H. Sequence-specific MR imaging findings that are useful in dating ischemic stroke. RadioGraphics 2012;32(5):1285-97; discussion 1297-1299.
5. Ghei SK, Zan E, Nathan JE, et al. MR imaging of hypoxic-ischemic injury in term neonates: pearls and pitfalls. RadioGraphics 2014;34(4):1047-1061.
6. Huang BY, Castillo M. Hypoxic-ischemic brain injury: imaging findings from birth to adulthood. RadioGraphics 2008;28(2):417-39; quiz 617.

7. Maurya VK, Ravikumar R, Bhatia M, Rai R. Hypoxic-Ischemic brain injury in an adult: magnetic resonance imaging findings. Armed Forces Med J India 2016;72(1):75-77.
8. Bartynski WS. Posterior reversible encephalopathy syndrome, part 1: fundamental imaging and clinical features. Am J Neuroradiol 2008;29(6):1036-1042.
9. Saposnik Gustavo, Barinagarrementeria Fernando, Brown Robert D., et al. Diagnosis and management of cerebral venous thrombosis. Stroke 2011;42(4):1158-1192.
10. Cartes-Zumelzu FW, Stavrou I, Castillo M, Eisenhuber E, Knosp E, Thurnher MM. Diffusion-weighted imaging in the assessment of brain abscesses therapy. Am J Neuroradiol 2004;25(8):1310-1317.
11. Wong AM, Zimmerman RA, Simon EM, Pollock AN, Bilaniuk LT. Diffusion-weighted MR imaging of subdural empyemas in children. Am J Neuroradiol 2004;25(6):1016-1021.
12. Fujikawa A, Tsuchiya K, Honya K, Nitatori T. Comparison of MRI sequences to detect ventriculitis. Am J Roentgenol 2006;187(4):1048-1053.
13. Mitchell BC, Dehkharghani S. Imaging of intracranial infectious diseases in adults. Appl Radiol 2014;43(2):6.
14. Buckle C, Castillo M. Use of diffusion-weighted imaging to evaluate the initial response of progressive multifocal leukoencephalopathy to highly active antiretroviral therapy: early experience. Am J Neuroradiol 2010;31(6):1031-1035.
15. Ukisu R, Kushihashi T, Tanaka E, et al. Diffusion-weighted MR imaging of early-stage Creutzfeldt-Jakob disease: typical and atypical manifestations. RadioGraphics 2006;26 (suppl 1):S191-204.
16. Yousem DM, Grossman RI. Neuroradiology: the requisites. Elsevier Health Sciences; 2010.
17. Chong-Han CH, Cortez SC, Tung GA. Diffusion-weighted MRI of cerebral toxoplasma abscess. Am J Roentgenol 2003;181(6):1711-1714.
18. Filippi CG, Edgar MA, UluğAM, Prowda JC, Heier LA, Zimmerman RD. Appearance of meningiomas on diffusion-weighted images: correlating diffusion constants with histopathologic findings. Am J Neuroradiol 2001;22(1):65-72.
19. Santelli L, Ramondo G, Della Puppa A, et al. Diffusion-weighted imaging does not predict histological grading in meningiomas. Acta Neurochir 2010;152(8):1315-9; discussion 1319.
20. Haldorsen IS, Kråkenes J, Krossnes BK, Mella O, Espeland A. CT and MR imaging features of primary central nervous system lymphoma in Norway, 1989-2003. Am J Neuroradiol 2009;30(4):744-751.
21. Huang W-Y, Wen J-B, Wu G, Yin B, Li J-J, Geng D-Y. Diffusion-weighted imaging for predicting and monitoring primary central nervous system lymphoma treatment response. Am J Neuroradiol 2016;37(11):2010-2018.
22. Hilario A, Ramos A, Perez-Nuñez A, et al. The added value of apparent diffusion coefficient to cerebral blood volume in the preoperative grading of diffuse gliomas. Am J Neuroradiol 2012;33(4):701-707.
23. Li W-B, Tang K, Chen Q, et al. MRI manifestions correlate with survival of glioblastoma multiforme patients. Cancer Biol Med 2012;9(2):120-123.
24. Given CA 2nd, Stevens BS, Lee C. The MRI appearance of tumefactive demyelinating lesions. Am J Roentgenol 2004;182(1):195-199.
25. Hyland M, Bermel RA, Cohen JA. Restricted diffusion preceding gadolinium enhancement in large or tumefactive demyelinating lesions. Neurol Clin Pract 2013;3(1):15-21.
26. Dutra BG, da Rocha AJ, Nunes RH, Maia ACM Júnior. Neuromyelitis optica spectrum disorders: spectrum of MR imaging findings and their differential diagnosis. RadioGraphics 2018;38(1):169-193.
27. Gluck L, Vollbracht S. Diffusion weighted imaging in a case of longitudinally extensive transverse myelitis in neuromyelitis optica. Neurology 2017;88(suppl 16):395.
28. Sarbu N, Shih RY, Jones RV, Horkayne-Szakaly I, Oleaga L, Smirniotopoulos JG. White matter diseases with radiologic-pathologic correlation. RadioGraphics 2016;36(5):1426-1447.
29. Dahnert WF. Radiology Review Manual. Lippincott Williams & Wilkins; 2017.
30. Howard SA, Barletta JA, Klufas RA, Saad A, De Girolami U. Best cases from the AFIP: osmotic demyelination syndrome. RadioGraphics 2009;29(3):933-938. doi:10.1148/rg.293085151
31. Ruzek KA, Campeau NG, Miller GM. Early diagnosis of central pontine myelinolysis with diffusion-weighted imaging. Am J Neuroradiol 2004;25(2):210-213.
32. Kang EG, Jeon SJ, Choi SS, Song CJ, Yu IK. Diffusion MR imaging of hypoglycemic encephalopathy. Am J Neuroradiol 2010;31(3):559-564.
33. Bathla G, Policeni B, Agarwal A. Neuroimaging in patients with abnormal blood glucose levels. Am J Neuroradiol 2014;35(5):833-840.
34. Chu K, Kang D-W, Kim H-J, Lee Y-S, Park S-H. Diffusion-weighted imaging abnormalities in Wernicke encephalopathy: reversible cytotoxic edema? Arch Neurol 2002;59(1):123-127.
35. Zuccoli G, Pipitone N. Neuroimaging findings in acute Wernicke's encephalopathy: review of the literature. Am J Roentgenol 2009;192(2):501-508.
36. Lo C-P, Chen S-Y, Lee K-W, et al. Brain injury after acute carbon monoxide poisoning: early and late complications. Am J Roentgenol 2007;189(4):W205-211.
37. Sener RN. Acute carbon monoxide poisoning: diffusion MR imaging findings. Am J Neuroradiol 2003;24(7):1475-1477.
38. Moore MM, Kanekar SG, Dhamija R. Ethylene glycol toxicity: chemistry, pathogenesis, and imaging. Radiol Case Rep 2008;3(1):122.
39. Blanco M, Casado R, Vázquez F, Pumar JM. CT and MR imaging findings in methanol intoxication. Am J Neuroradiol 2006;27(2):452-454.
40. Liu AY, Maldjian JA, Bagley LJ, Sinson GP, Grossman RI. Traumatic brain injury: diffusion-weighted MR imaging findings. Am J Neuroradiol 1999;20(9):1636-1641.
41. Arfanakis K, Haughton VM, Carew JD, Rogers BP, Dempsey RJ, Meyerand ME. Diffusion tensor MR imaging in diffuse axonal injury. Am J Neuroradiol 2002;23(5):794-802.
42. Kuo K-H, Pan Y-J, Lai Y-J, Cheung W-K, Chang F-C, Jarosz J. Dynamic MR imaging patterns of cerebral fat embolism: a systematic review with illustrative cases. Am J Neuroradiol 2014;35(6):1052-1057.
43. Tsuruda JS, Chew WM, Moseley ME, Norman D. Diffusion-weighted MR imaging of the brain: value of differentiating between extraaxial cysts and epidermoid tumors. Am J Roentgenol 1990;155(5):1059-65; discussion 1066-1068.
44. Chen S, Ikawa F, Kurisu K, Arita K, Takaba J, Kanou Y. Quantitative MR evaluation of intracranial epidermoid tumors by fast fluid-attenuated inversion recovery imaging and echo-planar diffusion-weighted imaging. Am J Neuroradiol 2001;22(6):1089-1096.
45. Hakyemez B, Aksoy U, Yildiz H, Ergin N. Intracranial epidermoid cysts: diffusion-weighted, FLAIR and conventional MR findings. Eur J Radiol 2005;54(2):214-220.
46. Naeini RM, Yoo JH, Hunter JV. Spectrum of choroid plexus lesions in children. Am J Roentgenol 2009;192(1):32-40.
47. Maekawa T, Hori M, Murata K, et al. Choroid plexus cysts analyzed using diffusion-weighted imaging with short diffusion-time. Magn Reson Imaging 2019;57:323-327.
48. Mendes A, Sampaio L. Brain magnetic resonance in status epilepticus: a focused review. Seizure 2016;38:63-67.
49. Hübers A, Thoma K, Schocke M, et al. Acute DWI reductions in patients after single epileptic seizures - more common than assumed. Front Neurol 2018;9:550.
50. Mazumdar A, Mukherjee P, Miller JH, Malde H, McKinstry RC. Diffusion-weighted imaging of acute corticospinal tract injury preceding Wallerian degeneration in the maturing human brain. Am J Neuroradiol 2003;24(6):1057-1066.
51. DeVetten G, Coutts SB, Hill MD, et al. Acute corticospinal tract Wallerian degeneration is associated with stroke outcome. Stroke 2010;41(4):751-756.

JAOCR at the Viewbox

Alex Martin, D.O., Timothy McKnight, D.O.

Beaumont Hospital, Farmington Hills, MI



Hyperdense Bihemispheric Anterior Cerebral Artery: An Uncommon Location of a Classic Imaging Finding

An 82-year-old woman presented to the emergency department with shortness of breath and personality changes. After being diagnosed with a pulmonary embolism, a head CT was ordered to evaluate for metastases and/or hemorrhage prior to starting anticoagulation.

An unenhanced head CT **(A)** showed increased attenuation of the anterior cerebral artery (**white arrow in A**). An unenhanced brain MRI **(B)** demonstrated restricted diffusion of the corpus callosum and bilateral frontal lobes in the distribution of the pericallosal arteries **(solid arrow in B)**. Maximum intensity projection images from a CT angiogram **(C, D)** demonstrated a bihemispheric anterior cerebral artery (ACA) with abrupt cutoff of the common pericallosal artery **(black arrow in C)**, normal variant absent left A1 segment **(red arrow in D)**, and a hypoplastic left ACA arising from the right-sided circulation **(yellow arrow in D)**.

The hyperdense middle cerebral artery sign is a well-known finding of acute stroke on noncontrast CT and thought to represent direct visualization of the thrombus/embolus. A hyperdense vessel can also be caused by elevated hematocrit, atherosclerosis, pseudo-hyperdensity from decreased attenuation of the adjacent brain parenchyma, and dissection.[1]

The ACAs have numerous variations with the standard configuration seen in just over 50% of cases.[2] In the hemispheric ACA, the bilateral ACA territory is supplied by a single dominant A2 segment with hypoplasia of the contralateral A2 segment. This is in contrast to the azygous ACA in which a single A2 segment is supplied by two A1 segments.[1,2]

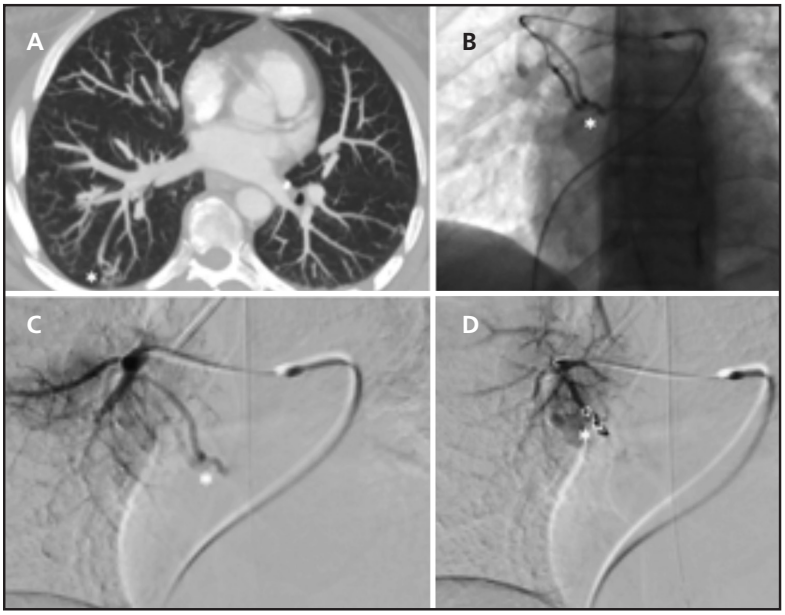
References

1. Rauch RA, Bazan C, Larsson EM, Jinkins JR. Hyperdense middle cerebral arteries identified on CT as a false sign of vascular occlusion. Am J Neuroradiol 1993;14(3):669-673.
2. Makowicz G, Poniatowska R, Lusawa M. Variants of cerebral arteries - anterior circulation. Pol J Radiol 2013;78(3):42-47.

JAOCR at the Viewbox

Mathieu Sabbagh, D.O.,[1] Donald von Borstel, D.O.[2]

[1]Department of Interventional Radiology, University of Arkansas for the Medical Sciences, Little Rock, AR
[2]Department of Radiology, Oklahoma State University Medical Center, Tulsa, OK



Hereditary Hemorrhagic Telangiectasia: A Review

A 56-year-old woman with a history of hereditary hemorrhagic telangiectasia (HHT) and positive for endoglin gene mutation presented with worsening hypoxia requiring mechanical ventilation secondary to right-to-left shunting from pulmonary arteriovenous malformations (AVMs). Interventional radiology was consulted for further evaluation and treatment with angiogram and embolization.

Initial CT angiogram demonstrated multiple pulmonary AVMs including those in the right lower lobe (*asterisk* in **Figure A**). The patient underwent pulmonary angiography that demonstrated concordant findings to the cross-sectional imaging (*asterisks* in **Figure B and C**). Coil embolization of the AVMs was performed. A post-interventional digitally subtracted angiogram (**Figure D**) displayed coil embolization of the right lower lobe pulmonary AVM (*asterisk*). Following intervention, the patient's hypoxia improved, and she was weaned off mechanical ventilation to oxygen via nasal cannula and was discharged home.

Hereditary hemorrhagic telangiectasia, also known as Osler-Weber-Rendu syndrome, is an autosomal dominant disease manifested by AVMs and telangiectasia. Prevalence of HHT is 1 in 5000 to 10000. Clinical diagnosis is centered on the presence of 3 out of 4 Curacao criteria, which includes: recurrent epistaxis, skin and mucosal telangiectasia, visceral AVM, and family history of HHT. Three genes have been associated with HHT: endoglin, aktivin, and SMAD4.[1,2]

Pulmonary AVMs have a strong association with HHT due to a mutation in the endoglin gene. These AVMs are high-flow shunts that can cause hypoxia, dyspnea, and hemoptysis. Pulmonary AVMs put patients at risk of brain abscess and stroke. AVMs in the lungs are commonly found in the lower lobes and have the radiographic appearance of a pulmonary nodule or nidus with a large feeding artery and draining vein. Treatment of pulmonary AVMs with coil embolization should be considered when the feeding artery is > 3 mm.[1,2] In addition to the lungs, AVMs can also be seen elsewhere, including the central nervous system and gastrointestinal tract.

References

1. Carette MF, Nedelcu C, Tassart M, et al. Imaging of hereditary hemorrhagic telangiectasia. Cardiovasc Intervent Radiol 2009;32(4):745-757.
2. Meek ME, Meek JC, Beheshti MV. Management of pulmonary arteriovenous malformations. Semin Intervent Radiol 2011;28(1):24-31.